Annales Societatis Geologorum Poloniae (2020), vol. 90: 27–49 doi: https://doi.org/10.14241/asgp.2020.05

AGE CONSTRAINTS ON THE PRE-VARISCAN AND VARISCAN THERMAL EVENTS IN THE KAMIENIEC ZĄBKOWICKI METAMORPHIC BELT (THE FORE-SUDETIC BLOCK, SW POLAND)

Mirosław JASTRZĘBSKI[1*], Andrzej ŻELAŹNIEWICZ[1], Bartosz BUDZYŃ[2], Jiří SLÁMA[3] & Patrik KONEČNÝ[4]

[1] Institute of Geological Sciences, Polish Academy of Sciences, Research Centre in Wrocław, ul. Podwale 75, 50-449 Wrocław, Poland; e-mails: mjast@twarda.pan.pl, pansudet@pwr.edu.pl
[2] Institute of Geological Sciences, Polish Academy of Sciences, Research Centre in Kraków, ul. Senacka 1, 31-002 Kraków, Poland; e-mail: ndbudzyn@cyf-kr.edu.pl
[3] The Czech Academy of Sciences, Institute of Geology, Rozvojová 269, Prague 6, 16500, Czech Republic; e-mail: slama@gli.cas.cz
[4] Dionýz Štúr State Geological Institute, Mlynská dolina 1, SK-81704 Bratislava, Slovak Republic; e-mail: patrik.konecny@geology.sk
** Corresponding author*

Jastrzębski, M., Żelaźniewicz, A., Budzyń, B., Sláma, J. & Konečny, P., 2020. Age constraints on the Pre-Variscan and Variscan thermal events in the Kamieniec Ząbkowicki Metamorphic belt (the Fore-Sudetic Block, SW Poland). *Annales Societatis Geologorum Poloniae,* 90: 27–49.

Abstract: The Kamieniec Ząbkowicki Metamorphic Belt (KZMB) is a narrow zone of mainly mica schists, subordinate acid metavolcanics and scarce eclogites, sandwiched between Brunovistulia and the northern tip of the Teplá-Barrandia microplates. Locally occurring high-pressure relics indicate subduction of the metasedimentary succession of the KZMB, the origin and provenance of which remain unclear. Laser ablation-inductively coupled plasma-mass spectrometry (LA-ICP-MS) investigations of detrital zircons show that the metapelites represent an Ediacaran-Cambrian sedimentary basin, with a maximum depositional age of 561±9 Ma. This basin was filled with detritus from a source or sources, composed of rocks containing zircons that are mainly Cryogenian-Ediacaran and Palaeoproterozoic in age. No younger component was found in the zircon population studied. The isotopic U-Pb LA-ICP-MS and chemical U-Th-total Pb electron probe microanalysis (EPMA) monazite geochronology data indicate an important regional tectono-metamorphic event at ca. 330 Ma. Though these data do not permit determination of the peak pressure from the peak temperature stages, the event was part of a complex collision of the Saxothuringian plate with Brunovistulia.

Key words: U-Pb geochronology, LA-ICP-MS dating, U-Th-total Pb geochronology, EPMA dating, microplates of the Bohemian Massif, Kamieniec Ząbkowicki Metamorphic Belt, Variscan metamorphism.

Manuscript received 25 March 2020, accepted 1 June 2020

INTRODUCTION

In the northeasternmost Bohemian Massif, there is a narrow belt of mica schists ca. 10 km wide, referred to as the Kamieniec Ząbkowicki Metamorphic Belt (KZMB); on the basis of zircon data collected from the adjacent units, it is assigned to the Saxothuringian microplate (Oberc-Dziedzic *et al.*, 2018). The KZMB is positioned between the northwestern margin of the Brunovistulian terrane and the Góry Sowie Massif. The latter has been considered to be the northeast continuation of the Teplá-Barrandia/Bohemia Terrane (Matte *et al.*, 1990; Franke and Żelaźniewicz, 2000; Oberc-Dziedzic *et al.*, 2015), the Central Sudetic Terrane (Cymerman *et al.*, 1997) the Góry Sowie–Kłodzko Terrane (Mazur *et al.*, 2006) or the Central Sudetic Accretionary Wedge (Mazur *et al.*, 2015). In the regional subdivision, this narrow, N–S-trending belt belongs to the Fore-Sudetic Block and stretches from Kamieniec Ząbkowicki towards Wrocław, though it is extensively hidden under the Cenozoic cover (Fig. 1A).

The mylonitized gneisses of the Góry Sowie Massif (e.g., Dziedzicowa, 1979; Żelaźniewicz, 1995), schistose rocks of the Niemcza Shear Zone (Dziedzicowa, 1975, 1985; Mazur and Puziewicz, 1995; Żelaźniewicz, 1995; Klimas *et al.*, 2003), mica schists of the Kamieniec Ząbkowicki Metamorphic Belt (e.g., Dziedzicowa, 1979; Mazur and Józefiak, 1999) and para- and orthogneisses of the Strzelin Massif (e.g., Oberc-Dziedzic *et al.*, 2005; 2015) occur along a W–E transect (Fig. 1B). In the vicinity of Kamieniec Ząbkowicki, there are outcrops of porphyroblastic garnetiferous mica schists with high-pressure relicts (Nowak, 1998; Szczepański *et al.*, 2018) and lenses of eclogites, metamorphosed at ca. 13–15 kbar and 600°C (Achramowicz *et al.*, 1997). The high-pressure (HP) signatures in these rocks emphasize the geodynamic importance of the whole belt in the eastern Variscides. However, so far neither the pre-Variscan nor the Variscan events recorded in these rocks have been constrained by isotopic geochronology.

Eclogites set in mica schists near Kamieniec Ząbkowicki are not unique in this part of the Bohemian Massif. However, such rocks are only confined to a broad, N–S-trending border area between the Saxothuringian and Moravo-Silesian (Brunovistulia) Zones. In the latter, the Velké Vrbno Dome contains eclogite (metamorphosed at 14–17 kbar, 600––700 °C) lenses, associated with orthogneiss and embedded in a metavolcanic suite (Štípská *et al.*, 2006). On the other hand, gneisses of the Orlica-Śnieżnik Dome to the south of the Sudetic Marginal Fault (Fig. 1) that contain eclogites (15–30 kbar, 670–930 °C) in the Śnieżnik area (e.g., Bakun-Czubarow, 1998; Štípská *et al.*, 2012; Majka *et al.*, 2019) are assigned to Saxothuringia (e.g., Franke *et al.*, 1993; Franke and Żelaźniewicz, 2000).

The aim of this study of metapelites in the KZMB is to specify the provenance and terrane affiliation of this belt The authors constrained the detrital zircon age spectrum and the maximum depositional age of the sedimentary protolith. Furthermore, timing constraints on the age of regional metamorphism in the KZMB were established using isotopic Laser ablation-inductively coupled plasma-mass spectrometry (LA-ICP-MS) U-Pb dating and "chemical" U-Th-total Pb electron probe microanalysis (EPMA) dating. The age results obtained provided new data on the position and significance of the provenance, protolith and metamorphic age records in mica schists of the KZMB in pre-Variscan and Variscan times. These age data are of significant importance in refining knowledge of the evolution of the northeastern part of the Bohemian Massif and the Fore-Sudetic Block, in particular.

GEOLOGICAL SETTING

The KZMB occurs in the eastern part of the Fore-Sudetic Block. It emerges from beneath Cenozoic deposits in a N–S-trending belt, partly outcropping between Łagiewniki and Kamieniec Ząbkowicki (Fig. 1B). The belt is composed mainly of mica schists with minor intercalations of quartzo-feldspathic rocks, quartzo-graphitic schists, marbles, amphibolites (Dziedzicowa, 1979; Józefiak, 1998; Nowak, 1998) and eclogites localized only in its southern part (Achramowicz *et al.*, 1997). Microfossils found in the quartzites and mica schists indicate their Ediacaran to earliest Cambrian protolith age (Gunia, 1979).

The KZMB underwent a polyphase tectonic history (Achramowicz, 1994; Nowak, 1998; Mazur and Józefiak, 1999; see Gurgurewicz and Bartz, 2011 for review), which was accompanied by regional metamorphism. The clockwise P-T path reconstructions, elaborated so far for the KZMB mica schists, are roughly comparable. In the mica schists, pseudomorphs after HP lawsonite (Nowak, 1998) occasionally have been observed. The conditions of the early HP episode were estimated as 11–12 kbar and 400–430 °C (Nowak, 1998). Recent thermodynamic modelling indicates that the Kamieniec mica schists may have experienced pressures twice as high, reaching 20–25 kbar at 520 °C (Szczepański *et al.*, 2018). Peak temperature conditions in mica schists from different parts of the KZMB range from

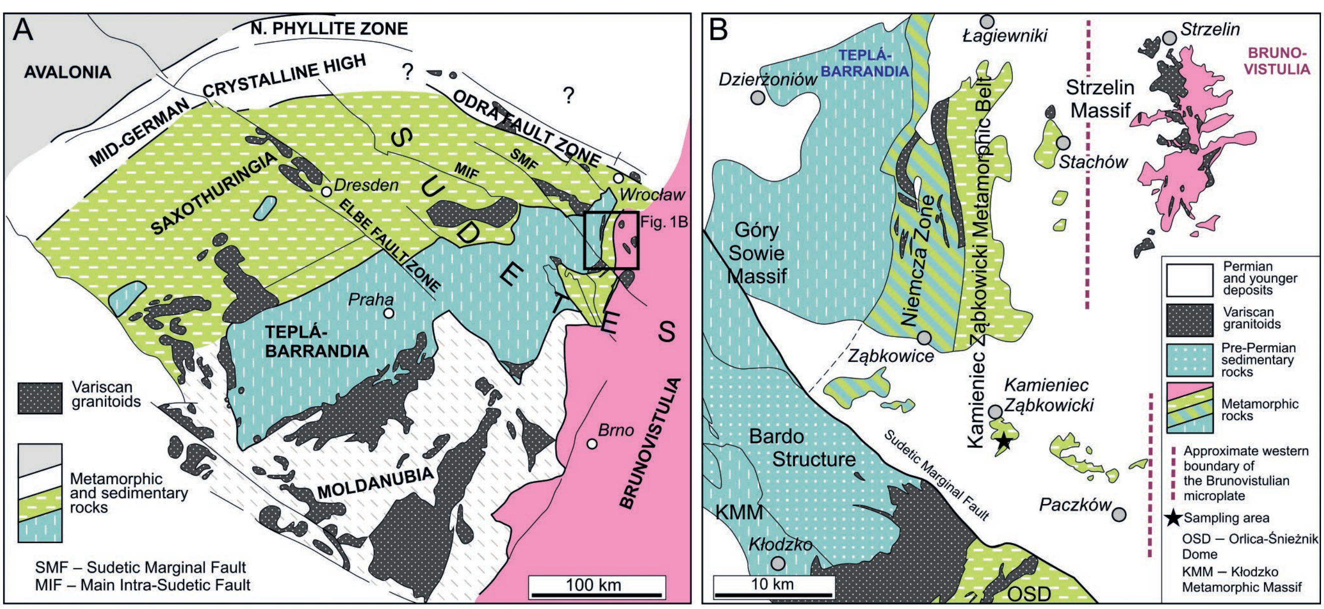

Fig. 1. Microplates (terranes) in the Bohemian Massif and the Fore-Sudetic Block. **A.** Microplate (terrane) boundaries in the Bohemian Massif (after Oberc-Dziedzic *et al.*, 2015). **B.** Geological map of the eastern part of the Fore Sudetic Block with location of the microplate boundaries (compiled after Sawicki, 1965 and Oberc-Dziedzic *et al.*, 2018).

500 °C to 640 °C with pressures of 3–10 kbar (see Józefiak, 1998; Nowak, 1998; Szczepański *et al.*, 2018). Such a wide scatter of P-T estimates indicates a tectonic shuffling of rock units metamorphosed at different depths (Mazur and Józefiak, 1999). A series of thrust sheets with westward-increasing metamorphic grade was reported within the belt (Achramowicz *et al.*, 1997; Nowak, 1998; Mazur and Józefiak, 1999).

An age of metamorphism of the KZMB was so far inferred indirectly from relationships with the adjacent units. In the northern part of the KZMB, some Niemcza granitoid bodies intruded the boundary zone between the Niemcza Shear Zone and KZMB at 335±2 Ma (U-Pb LA-ICP-MS zircon dating; Pietranik *et al.*, 2013). Several other studies of the Niemcza granodiorites persistently indicate an age of ca. 340–330 Ma (Oliver *et al.*, 1993; Kröner and Hegner, 1998; Kennan *et al.*, 1999), interpreted as the time of their syntectonic intrusion.

ANALYTICAL METHODS

The mica schists cropping out near Kamieniec Ząbkowicki (50°31'06"N, 16°53'13"E) were sampled for this study (samples SUD24/1 and SUD24/2). The mica schists are porphyroblastic, coarse-grained rocks bearing large porphyroblasts of garnet (up to 1.0 cm in diameter) with chloritoid, quartz, muscovite, margarite and rutile inclusions. Rhomboidal pseudomorphs of phases that replaced lawsonite, similar to those described by Nowak (1998), occur in garnet cores in sample SUD24/1 (Fig. 2). Apart from relics of lawsonite, the rhomboidal inclusions contain paragonite, epidote, ilmenite, muscovite and kyanite. The rock matrix mainly consists of quartz, biotite, chlorite, staurolite and plagioclase. The parallel alignment of these minerals forms a penetrative schistosity. Zircon and monazite are accessory phases in each of the samples investigated.

Preliminary observations and sample selection for monazite dating were performed using a JEOL SuperProbe JXA–8230 Electron Probe Microanalyzer (EPMA) equipped with five wavelength dispersive spectrometers in the Laboratory of Critical Elements, AGH–KGHM (AGH University of Science and Technology, Kraków, Poland). A SUD24/1 mica schist sample containing monazite grains with sizes sufficient for placing laser ablation spots was selected for LA-ICP-MS U-Pb dating, whereas a SUD24/2 sample with smaller grains was selected for EPMA U-Th-total Pb dating. The composition of the monazites in both samples was measured using EPMA.

Compositional analyses of monazite were conducted using a Cameca SX 100 EPMA equipped with 4 wavelength spectrometers, at the Laboratory of Electron Microanalysis, Geological Institute of Dionýz Štúr (Department of Special Laboratories, Bratislava, Slovak Republic). The analyzes were performed using 15 kV accelerating voltage, 180 nA sample current and 3 µm beam diameter (see Konečný *et al.*, 2018 for analytical protocol and further details). The calculation of individual monazite dates in the SUD24/2 sample was processed using the in-house DAMON software (P. Konečný, unpublished); the mean age of the monazite population was calculated using Isoplot v. 4.16 (Ludwig, 2012).

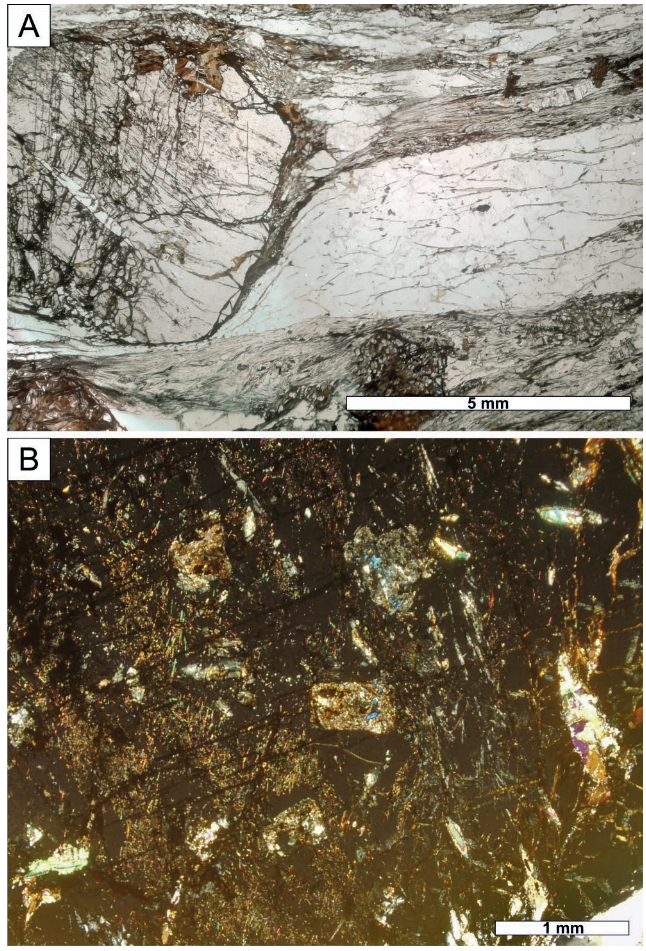

Fig. 2. Petrography of the mica schists studied. **A**. In the core of a garnet porphyroblast, chloritoid, quartz, margarite and rutile define the early metamorphic fabric. The external fabric is defined by alternating quartz and mica-rich laminae. Plane-polarized light (SUD24/2). **B**. Garnet core included elongated quartz, rutile, white mica and rhomboidal pseudomorphs after lawsonite. Cross-polarized light (SUD24/1).

The zircon and monazite for further LA-ICP-MS U-Pb analysis were separated from sample SUD24/1 using standard techniques and handpicking under a binocular microscope. Zircon and monazite grains were mounted in epoxy resin and polished. Cathodoluminescence (CL) of zircons and back-scattered electron (BSE) images of zircons and monazites were performed prior to the LA-ICP-MS measurements. A Thermo Scientific Element 2 sector field ICP-MS coupled to a 193 nm ArF excimer laser (Teledyne Cetac Analyte Excite laser) at the Institute of Geology of the Czech Academy of Sciences, Prague, Czech Republic, was used to measure the Pb/U and Pb isotopic ratios in zircon and monazite.

The laser was fired at a repetition rate of 5 Hz with fluence of 1.95 J/cm^2 and spot size of 10 microns for monazite analysis and 3.5 J/cm^2 and spot size of 25 microns for zircon analysis. The He carrier gas was flushed through the two-volume ablation cell at a flow rate of 0.85 L/min and mixed with 0.7 L/min Ar and 0.004 L/min N_2 prior to introduction into the ICP. The in-house glass signal homogenizer (design of Tunheng and Hirata, 2004) was used for mixing all the gases and aerosol, resulting in smooth, spike-free signal. The signal was tuned for maximum sensitivity of Pb and U and low oxide level (below 0.1% as measured at the beginning of the analytical session). Typical acquisitions consisted of a 15 second measurement of blank followed by measurement of U, Th and Pb signals from the ablated phosphates for another 35 seconds. A total of 420 mass scans were acquired in time resolved – peak jumping – pulse counting / analogue mode with 1 point measured per peak for masses ^{204}Pb + Hg, ^{206}Pb, ^{207}Pb, ^{208}Pb, ^{232}Th, ^{235}U, and ^{238}U. Owing to a non-linear transition between the counting and analogue acquisition modes of the ICP instrument and the fact that ^{238}U is usually measured in "both" mode, the raw data were pre-processed using a Python routine for decoding the Thermo Element ICPMS data files (Hartman *et al.*, 2017) and an in-house Excel macro. As a result, the intensities of ^{238}U were left unchanged if measured in a counting mode and recalculated from ^{235}U intensities if the ^{238}U was acquired in an analogue mode, thus eliminating the non-linearity between pulse-counting and analogue-detecting modes. Data reduction then was carried out off-line using the Iolite data reduction package version 3.4 with the VizualAge utility (Petrus and Kamber, 2012). Full details of the data reduction methodology can be found in Paton *et al*. (2010). The data reduction included correction for gas blank, laser-induced elemental fractionation of Pb and U and instrument mass bias. For the data presented here, blank intensities and instrumental bias were interpolated using an automatic spline function, while down-hole inter-element fractionation was corrected using an exponential function. No common Pb correction was applied to the data, owing to the high Hg contamination of the commercially available He carrier gas, which precludes accurate correction of the interfering ^{204}Hg on the very small signal of ^{204}Pb (common lead).

Residual elemental fractionation and instrumental mass bias of monazite analyses were corrected by normalization to the natural monazite sample from Jarasinga leptynite (India), with a TIMS U-Pb age of 953 ± 4 Ma (Aftalion *et al.*, 1991). The monazites Manangoutry (Madagascar, 555 ± 2 Ma; Paquette and Tiepolo, 2007) and Itambe (Brazil, $^{207}Pb/^{235}U$ age of 506.4 ± 0.7 Ma; Gonçalves *et al.*, 2016) were periodically measured for quality control. The obtained mean $^{207}Pb/^{235}U$ values of 553.1 ± 2.8 and 505.3 ± 2.3 Ma (2σ), respectively, are less than 1% within their published values. In line with the recommendations of Horstwood *et al*. (2016), the excess variance (Paton *et al.*, 2010) of the reference Jarasinga monazite was calculated in Isoplot and quadratically added to the measurement uncertainties of all unknowns as well as to all pooled ages (weighted average and U-Pb Concordia age as it is called in Isoplot).

Residual elemental fractionation and instrumental mass bias of zircon analyses were corrected by normalization to the natural zircon reference material Plešovice (Sláma *et al.*, 2008). The excess variance (Paton *et al.*, 2010) of the primary Plešovice zircon was calculated in Isoplot and quadratically added to the measurement uncertainties of all unknowns including validation zircon reference materials GJ-1 {nr. 63} (Jackson *et al.*, 2004) and 91500 (Wiedenbeck *et al.*, 1995). These two were analysed periodically during the measurement for quality control. The obtained values (GJ-1: concordia age of 603 ± 4 Ma (2σ); 91500: concordia age of 1068 ± 5 Ma (2σ)) correspond perfectly and are less than 1% accurate within the published reference values (GJ-1: $^{206}Pb/^{238}U$ age of 600.5 ± 0.4 Ma, Schaltegger *et al.*, 2015 and $^{207}Pb/^{206}Pb$ age of 608.53 ± 0.4 Ma, Jackson *et al.,* 2004 respectively; 91500: $^{207}Pb/^{206}Pb$ age of 1065.4 ± 0.3 Ma, Wiedenbeck *et al.*, 1995).

The U-Pb ages are presented as concordia (pooled) age and probability density plots, generated with the ISOPLOT program v. 4.16 (Ludwig, 2012).

RESULTS

Zircon geochronology

The oscillatory zoning and Th/U ratios >0.1 (except for one analysis) indicate an igneous origin of the zircons investigated (cf., Rubatto, 2017). Nighty eight U-Pb analyses with <10% discordance, out of 140 analyses performed (one analysis per grain), yielded ages broadly ranging from 3.34 Ga to 504 Ma (sample SUD24/1; Appendix 1). The detrital population is dominated by Neoproterozoic and Palaeoproterozoic grains (Figs 3, 4). The two oldest zircon ages recognized are Archean: 3.34 and 2.61 Ga. They were determined for the oscillatory zoned cores of ca. 100 µm anhedral zircon grains. The Palaeoproterozoic is represented by 16 anhedral zircons, variously structured (homogeneous to oscillatory zoned) and sized (70 to 200 µm), with ages ranging from 2.33 to 1.81 Ga. A single age of ca. 1.42 Ga came from the core of a small (70 µm long) zonal zircon. A minor cluster of 1089–722 Ma is formed by 12 small ca. 100–120 µm anhedral grains, usually bright in CL and oscillatory zoned. The major age cluster is of Cryogenian-Ediacaran age (696—547 Ma; n = 65). The Cryogenian- Ediacaran zircons are subhedral to anhedral grains, 70 to 250 µm in diameter that exhibit predominantly oscillatory zoning and, occasionally, sector zoning. Two younger ages (521 and 504 Ma) have been obtained from small, subhedral zircons ca. 70–80 µm long, showing an oscillatory zoned structure (Figs 3A, C, 4; Appendix 1). The maximum depositional age of the protolith of the investigated mica schist, calculated using five youngest $^{206}Pb/^{238}U$ ages (discordance ≤ 3%) that overlap within error (2σ) with the youngest age, is 560.9±9.1 Ma (MSWD = = 0.83, probability of concordance 0.36). No younger component has been found in the zircon population studied.

Monazite composition and age data

Monazite in both mica schists investigated (SUD24/1 and SUD24/2) is present as anhedral grains in the rock matrix, with sizes from several to ca. 60 µm and commonly forming aggregates. Individual monazite grains up to ca. 100 µm are present in the SUD24/1 sample. Rare, small inclusions of monazite in garnet also occur, but these are too small for accurate EPMA measurements. Monazite grains are homogeneous or, rarely, demonstrate growth or patchy zoning. The composition varies significantly within the monazite

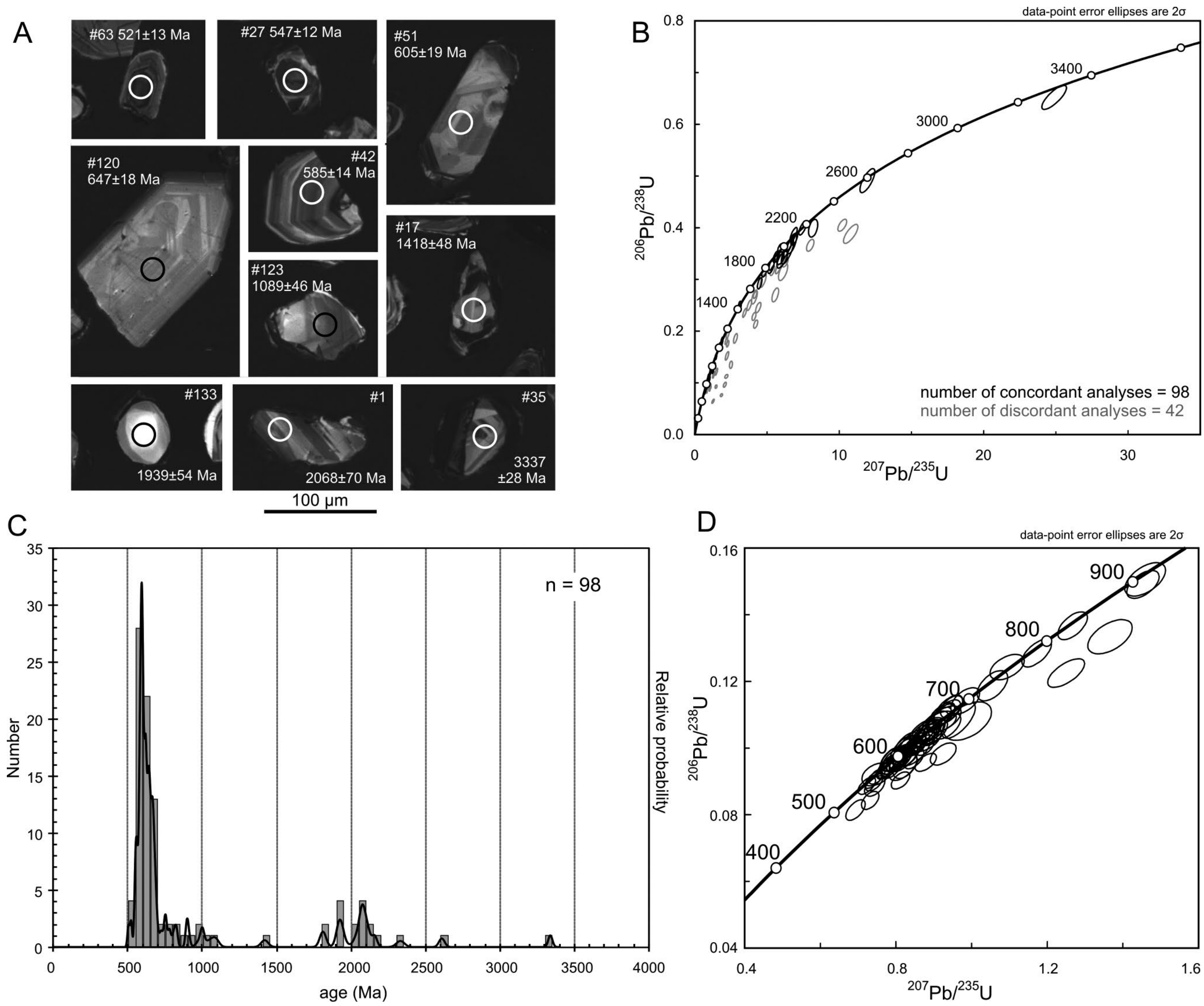

Fig. 3. Results of U-Pb LA-ICP-MS zircon dating. **A.** Cathodoluminescence images and LA-ICP-MS ages of selected zircons from the Kamieniec Ząbkowicki Metamorphic Belt (sample SUD24/1). Scale bar under CL images (100 µm) refer to all zircon grains. Spot labels correspond to labels in Appendix 1. **B.** Concordia U-Pb plot. Analyses with discordance >10% are indicated by grey ellipses. **C.** Probability density plot; $^{206}Pb/^{238}U$ ages are given for data <1 Ga, $^{207}Pb/^{206}Pb$ ages are given for data >1Ga. **D.** Concordia U-Pb plot in Neoproterozoic / Early Palaeozoic range. Analyses with discordance <10%.

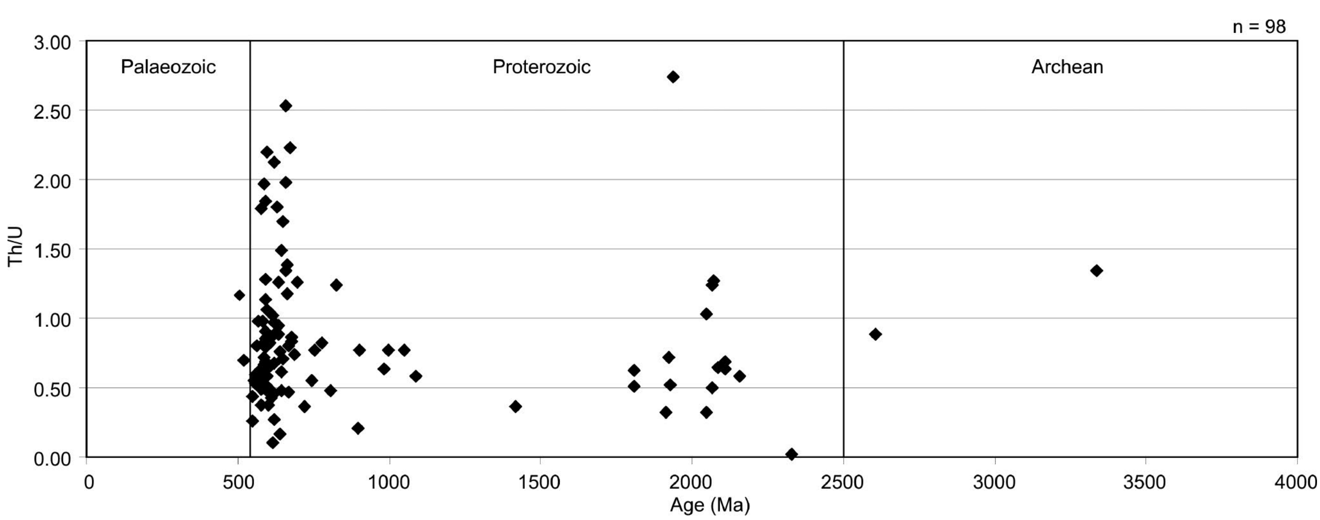

Fig. 4. Distribution of U-Pb ages *vs.* Th/U ratio in detrital zircons in mica schists SUD42/1.

population, including 1.58–9.44 wt.% ThO_2, 0.24–1.31 wt.% UO_2, 24.40–30.09 wt.% Ce_2O_3 in SUD24/1 and 3.07–16.37 wt.% ThO_2, 0.11–1.48 wt.% UO_2, 21.23–30.01 wt.% Ce_2O_3 in SUD24/2 (Appendix 2).

The isotopic U-Pb measurements in 8 grains (1–3 analyses per grain) from sample SUD24/1 demonstrated considerable discordance, indicating the presence of common Pb, which is rare for monazite (Fig. 5E;

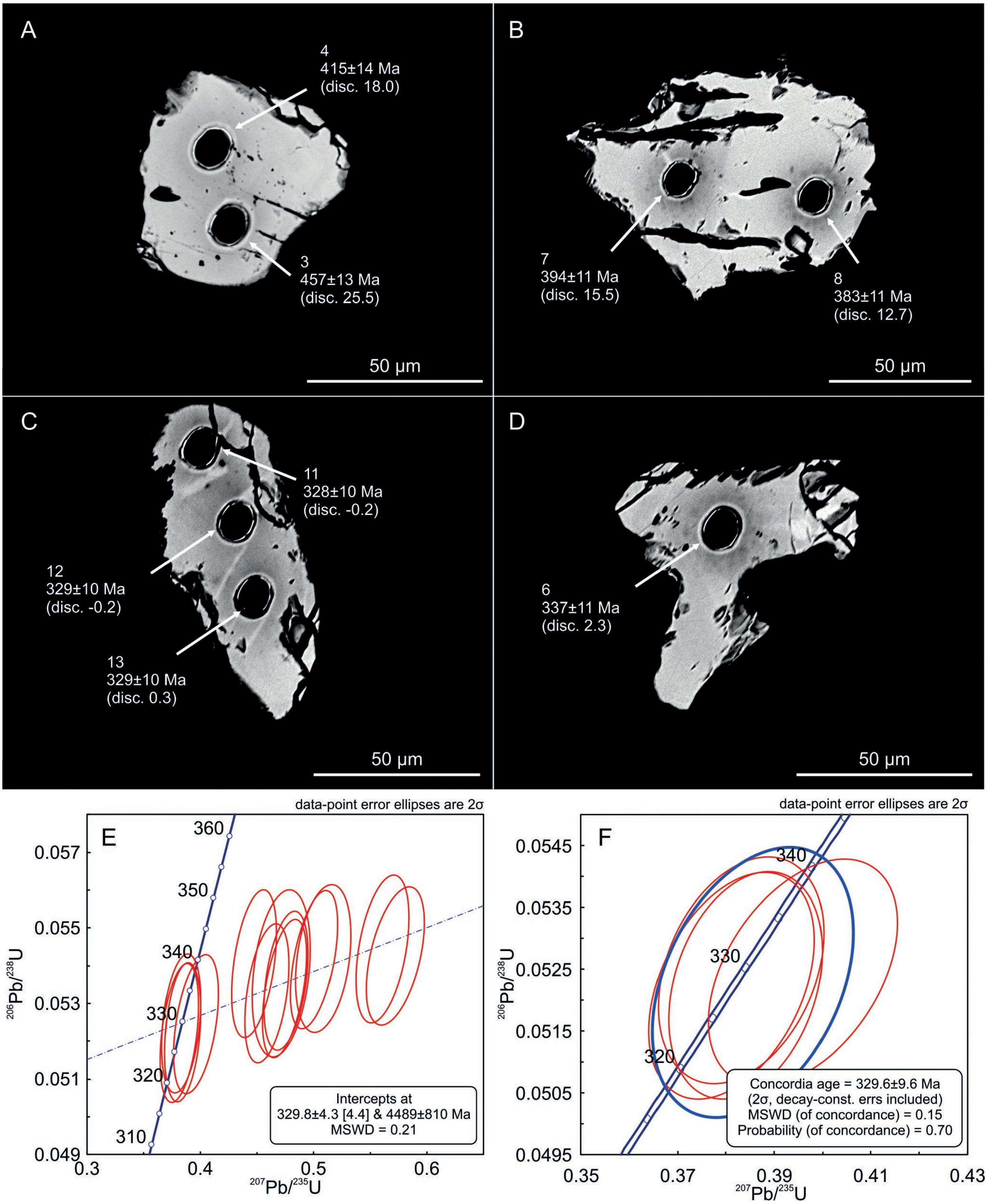

Fig. 5. Results of U-Pb LA-ICP-MS monazite dating. **A–D**. Representative BSE images BSE images of monazite separated from the mica schist sample SUD24/1. Spot labels correspond to labels in Appendix 3. **E–F**. Results of isotopic LA-ICP-MS U-Pb analyses; $^{207}Pb/^{235}U$ dates are given in (Ma), discordance is given in (%). See text for further details.

Appendix 3). The lower intercept at 329.8±4.3 Ma (MSWD = = 0.21, n = 13; Fig. 5E) is the same as an U-Pb Concordia age of 329.6±9.6 Ma (2σ, MSWD = 0.15; Fig. 5F) yielded by four analyses with a discordance from -0.2 to +2.3%. Monazite in SUD24/2 sample yielded individual U-Th-total Pb dates from ca. 318 to 391 Ma (Appendix 4), with a mean age of 330±5 (2σ, MSWD = 0.57, n = 36, Fig. 6C). The Th*-Pb isochron trend indicates minor Pb loss within the monazite population, rather than the presence of common Pb (Fig. 6D). Because “chemical” age data were obtained mostly in small grains and there is no robust method to constrain the presence of common Pb or Pb loss in individual grains, these results should be viewed with caution. However, an agreement between the U-Pb Concordia and U-Th-total Pb mean ages partially suggest that the latter also can be used in further interpretations.

DISCUSSION

The zircon age data demonstrate that the detrital age spectra of the Kamieniec Ząbkowicki mica schists are dominated by two age clusters, Neoproterozoic and Palaeoproterozoic, with the predominance of Ediacaran ages (Figs 3, 4). The latter indicate that the protolith of the mica schists studied was deposited in a sedimentary basin with supply from source areas dominated by Ediacaran crystalline rocks.

The zircon data provide new insights into the provenance of the high-pressure mica schists of the KZMB. The source areas were composed mainly of Neoproterozoic, predominantly Ediacaran to Cryogenian, igneous rocks with a less common Palaeoproterozoic component. The zircon age spectrum is similar to those known from Saxothuringia, derived from the West African Craton in Gondwana (Linnemann *et al.*, 2007, 2014; Fig. 7A). In the Sudetes, such detrital zircon age spectra were found in metasedimentary rocks of the Lusatian and Izera-Karkonosze massifs (e.g., Linnemann *et al.*, 2007, 2014; Żelaźniewicz *et al.*, 2009; Oberc-Dziedzic *et al.*, 2010a; Žáčková *et al.,* 2012), metavolcanosedimentary rocks of the Kaczawa Fold Belt (Kryza *et al.,* 2007; Kryza and Zalasiewicz, 2008; Tyszka *et al.*, 2008), paragneisses, mica schists and quartzites of the Orlica-Śnieżnik Dome (Jastrzębski *et al.*, 2010, 2015; Mazur *et al.*, 2012, 2015), quartzites of the Staré Město Belt (Jastrzębski *et al.*, 2015) and also in some paragneisses of the Strzelin Massif (Oberc-Dziedzic *et al.,* 2018). Such zircon age characteristics are also very similar to that in the Erzgebirge region of the Saxothuringian plate (Collett *et al.*, 2020 and references therein). In the adjacent northern part of Brunovistulia (the Strzelin Massif and Silesian Domain of the Moravo-Silesian Zone), rocks contain significant amount of 1.4 Ga zircons and for this reason they are expected to have been derived from the Amazonian part of Gondwana (Oberc-Dziedzic *et al.*, 2003; Żelaźniewicz *et al.*, 2005; Mazur *et al.*, 2010). In the Kamieniec Ząbkowicki metapelites, a single analysis of ca. 1418 Ma (Appendix 1) was obtained in the narrow core of a zoned grain (Fig. 3A). An interpretation that the KZMB sedimentary basin was located within the delivery reach of the detritus, ultimately derived from rocks similar to those of the Rondonia province in Amazonia, would not be well founded (Figs 3, 4).

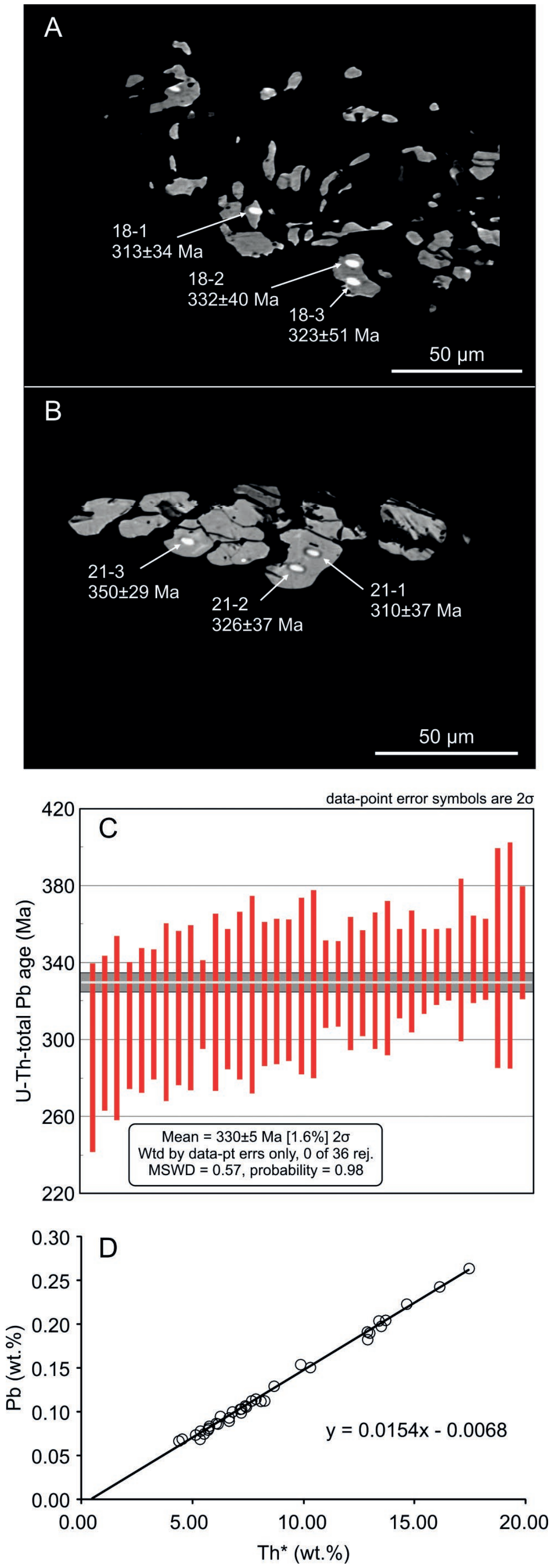

Fig. 6. U-Th-total Pb EPMA monazite dating. **A–B**. BSE images of monazite grains from the mica schist SUD24/2. Analytical spot labels correspond to analysis labels in Appendix 4; dates are given in (Ma). **C–D**. Results of U-Th-total Pb dating. Th* values denote measured Th plus U converted to hypothetical Th with respect to production of the equivalent amount of radiogenic Pb (Konečný *et al.*, 2018). Negative value of isochron intercept with Pb axis indicates minor Pb loss in monazite population.

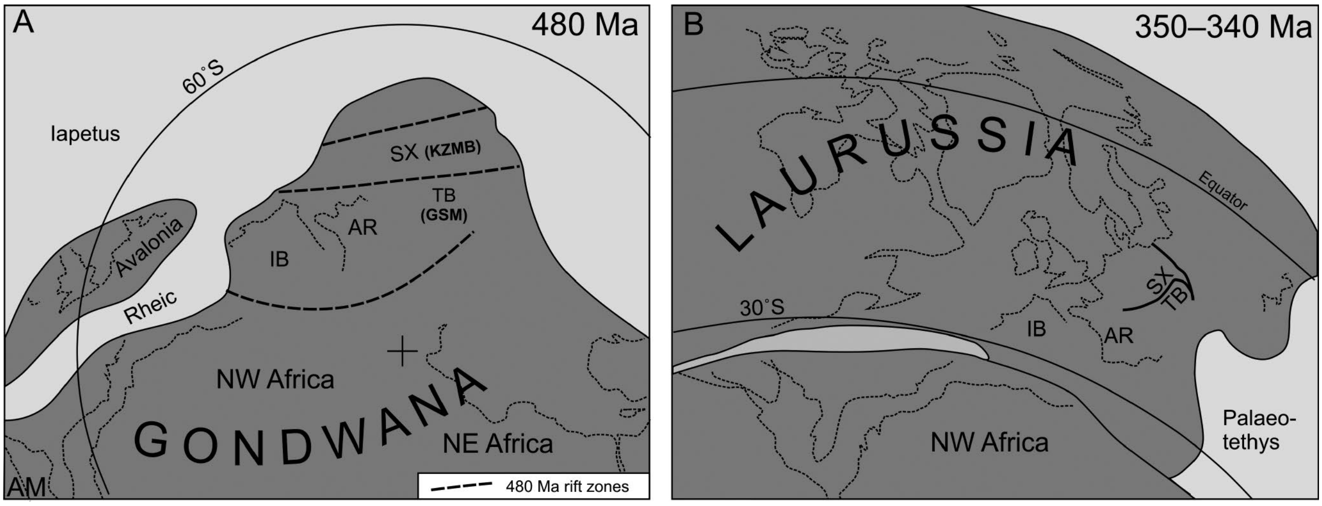

Fig. 7. Position of the Kamieniec Ząbkowicki Metamorphic Belt during the Early and Late Palaeozoic on palaeogeographic schemes modified after Franke *et al.* (2017). **A.** Gondwana before the Early Ordovician fragmentation. **B.** Variscan terranes during the Early Carboniferous. AM – Amazonia, IB – Iberia, AR – Armorica, SX – Saxothuringia, KZMB – Kamieniec Ząbkowicki Metamorphic Belt, TB – Teplá-Barrandia, GSM – Góry Sowie Massif.

However, a statistically more important group, defined by the 1089–722 Ma age cluster (n = 12), indicates a Grenvillian component, the presence of which cannot be easily reconciled with a source on the West African Craton. This requires seeking the Grenvillian or other source(s) with similar timing in nearby fragments of Rodinia/Gondwana. In Amazonia, anorogenic granites of Rondonia were emplaced at 990–900 Ma (Dall'Agnol *et al.*, 1987). On the other hand, in southern Scandinavia, the Sveconorwegian (1.14–0.90 Ga) events were followed by the abortive break-up of Rodinia around 850 Ma (Paulsson and Andréasson, 2002), which corresponds to the Tonian group of zircons identified in the mica schists investigated. Clearly more work has to be done to expand the age dataset of detrital zircons and shed more light on the provenance of the region studied.

A West African Craton affinity of the KZMB rocks is still the most probable, as their zircon age spectra are practically without Mesoproterozoic ages. It has to be noted that a true depositional age of the protolith may be younger than the calculated maximum depositional age of 560.9±9.1 Ma (cf., Cawood *et al*., 2012). Sedimentation of the protoliths of the mica schists of the KZMB thus probably commenced in the Ediacaran, but the onset of deposition in the Cambrian cannot be excluded.

Most of the detrital zircons reveal Th/U ratio >0.1 characteristic for igneous rocks (e.g., Rubatto, 2017). Zircons with Th/U ratio <0.1 are scarce (Fig. 4), so that no distinct metamorphic episode in the source area of the sedimentary basin can be distinguished. Nevertheless, the presence of 30% of U-Pb ages highly (>10%) discordant (Fig. 3B; not considered and not shown in the histogram on Figure 3C) indicates partial Pb loss in the detrital zircon population. The zircons investigated demonstrate no record of post-depositional metamorphic regrowth (Figs 3, 4).

The LA-ICP-MS U-Pb isotopic and EPMA U-Th-total Pb dating revealed that all the monazites investigated represent a ca. 330 Ma Carboniferous thermal event with no inherited ages. In the NE Bohemian Massif, such Early Carboniferous ages are common in tectonostratigraphic units that belong to both the Saxothuringian Zone and also to the Moldanubian Zone. Compared to geochronological data from the Saxothuringian units adjacent to the KZMB, ages of about 330 Ma generally are related to cooling or later thermal overprints. In metamorphic rocks of the Orlica-Śnieżnik Dome, Ar-Ar mica ages point to more protracted cooling between ~340 Ma and 320 Ma (Marheine *et al*., 2002; Schneider *et al*., 2006; for most recent reviews of geochronology of this unit see Skrzypek *et al*., 2017; Walczak *et al*., 2017 and Jastrzębski *et al*., 2019). On the other hand, the ca. 330 Ma monazite-forming event in the KZMB is generally 10–30 Myr. older than the late Variscan thermal event in the NW Brunovistulia (Szczepański, 2002; Schulmann *et al*., 2014). The monazite age of ca. 330 Ma also contrasts with Devonian ages obtained in the Góry Sowie Massif (Teplá-Barrandia), the tectonothermal evolution of which was accomplished much earlier, i.e., before ca. 360 Ma (van Breemen *at al*., 1988; O'Brien *et al.*, 1997; Bröcker *et al.*, 1998; Kryza and Fanning, 2007).

The zircon and monazite data altogether indicate that the KZMB mica schists and eclogites cannot be assigned either to Brunovistulia or to Teplá-Barrandia. Instead, the KZMB is geotectonically more compatible with the Orlica-Śnieźnik Dome, although the relevant rock complexes cannot be correlated directly across the Sudetic Marginal Fault because the tectonostratigraphic units in its walls represent different erosional levels over a vertical distance of some five kilometres (e.g., Cwojdziński and Żelaźniewicz, 1995). Both the Orlica-Śnieżnik Dome and the KZMB most probably can be assigned to the Saxothuringian microplate (e.g., Franke and Żelaźniewicz, 2000; Chopin *et al*., 2012; Oberc-Dziedzic *et al*., 2015). However, it should be noted that some geotectonic models consider these rocks as part of the Moldanubian microplate, which played an active role during the Variscan collision (e.g., Matte *et al.*, 1990). Both Saxothuringia and Moldanubia have West African connections and were adjacent in pre-Variscan times (Žák & Sláma, 2018); thus, the Moldanubian affinity of the KZMB cannot be excluded entirely.

Given the tectonic shuffling of rocks with different P-T records (Józefiak, 1998; Nowak, 1998) within the KZMB, the data of the present authors confirm that the belt can be interpreted as part of the edifice stacked by collision that developed between the northern tip of the Teplá-Barrandian/Bohemian terrane and the Brunovistulian terrane, as observed along the W-E transect from the Góry Sowie Massif to the Strzelin Massif (Fig. 1B). The KZMB (10–20 km outcrop breadth) is a narrow strip of an accretionary prism forced between two microcontinents, of which Brunovistulia represents the lower plate. Saxothuringia and the structurally higher Teplá-Barrandian/Bohemian terrane are in the upper plate. The original contact of these two terranes was later strongly modified by sinistral strike-slip tectonics, localized mainly in the Niemcza Shear Zone (Mazur and Puziewicz, 1995; Żelaźniewicz, 1995) that also embraced dismembered fragments of the Sudetic ophiolite (Fig. 1B).

Metapelites of the KZMB, with the revealed "Saxothuringian" detrital zircon age spectra, may be interpreted as a fragment of Ediacaran–Cambrian (?) successions, characteristic of the Saxothuringian margin (Oberc-Dziedzic *et al.*, 2018 for review), which was subducted to a depth of 40–50 km and involved in the Variscan belt in front of the Brunovistulian sector of Laurussia (Fig. 7B). In the KZMB, the main monazite-forming event occurred during regional metamorphism around 330 Ma, yet whether this took place at the HP stage or during exhumation remains unknown. In the belt, regional metamorphism was enhanced by an increased heat flow, concurrent with Mississippian granitic intrusions in the neighbouring unit, namely granodiorites in the Niemcza Shear Zone (Oliver *et al.*, 1993; Pietranik *et al.*, 2013) and tonalites emplaced in the Neoproterozoic (Brunovistulian) basement of the Strzelin Massif (Oberc-Dziedzic *et al.*, 2010b). The Niemcza granodiorite/monzodiorite crystallized from a magma within a temperature range of 850–730 °C and pressure of 4 ± 1 kbar (Puziewicz, 1992), thus at depths similar to those, at which the KZMB schists and eclogites re-equilibrated at the temperature peak on a clockwise P-T path (Dziedzicowa, 1979; Nowak, 1998; Szczepański *et al.*, 2018). The new data in the present account show that a rather complex amalgamation of rock units with different grades, which belong to the tectonic stack of Teplá-Barrandia/Bohemia, Saxothuringia and Brunovistulia, in the NE corner of the Bohemian Massif, took place in Mississippian times, mainly during the Viséan.

CONCLUSIONS

1. The maximum depositional age for the protolith of the metasedimentary rocks of the Kamieniec Ząbkowicki Metamorphic Belt is 560.9±9.1 Ma.
2. The predominance of zircon ages clustering in 1.09–0.55 Ga and 2.16–1.81 Ga, with only scarce Mesoproterozoic and Cambrian zircon ages, indicates that the source areas for the KMZB metapelites may have been in the West African Craton, as was the case for other parts of the Saxothuringia microplate.
3. The U-Pb and U-Th-total Pb monazite age data indicate that the metamorphism of the mica schists investigated occurred during the Viséan-earliest Serpukhovian (ca. 330 Ma) and can be related to tectonic extrusion of the Saxothuringian rocks along western Brunovistulia.

Acknowledgements

This study was financed by the National Science Centre, Poland through Grant No. 2014/15/B/ST10/03938. The work of Jiří Sláma was financed by institutional support to the Institute of Geology, ASCR, RVO 67985831. Gabriela Kozub-Budzyń is acknowledged for assistance with the EPMA measurements. Łukasz Kruszewski helped to identify mineral phases. Aleksandra Jaźwa, Izabella Kocjan and Anna Zagórska are thanked for the zircon and monazite separation. We also thank Józef Nowak for preparing the thin sections and Marek Śliwiński for assistance in processing the zircon data. The constructive reviews by Stephen Collett and an anonymous reviewer are gratefully acknowledged. Stanisław Mazur is thanked for careful editorial handling.

REFERENCES

Achramowicz, S., 1993. Paleostress in the country rocks to the Strzelin grainitoids from the analysis of dilational centrifugal structures, SW Poland. *Annales Societatis Geologorum Poloniae*, 63: 265–332. [In Polish, with English summary.]

Achramowicz, S., Muszyński, A. & Schliestedt, M., 1997. The northeasternmost eclogite occurrence in the Saxothuringian Zone, West Sudetes (Poland). *Chemie der Erde*, 57: 51–61.

Aftalion, M., Bibikova, E. V., Bowes, D. R., Hopgood, A. M. & Perchuk, L. L., 1991. Timing of early Proterozoic collisional and extensional events in the granulite-gneiss-charnockite-granite complex, Lake Baikal, USSR: a U-Pb, Rb-Sr, and Sm-Nd isotopic study. *Journal of Geology,* 99: 851–861.

Bakun-Czubarow, N., 1998. Ilmenite-bearing eclogites of the West Sudetes – their geochemistry and mineral chemistry. *Archiwum Mineralogiczne*, 51: 29–110.

Bröcker, M., Żelaźniewicz, A. & Enders, M., 1998. Rb-Sr and U-Pb geochronology of migmatitic gneisses from the Góry Sowie (West Sudetes, Poland): the importance of Mid-Late Devonian metamorphism. *Journal of Geological Society, London,* 155: 1025–1036.

Cawood, P. A., Hawkesworth, C. J. & Dhuime, B., 2012. Detrital zircon record and tectonic setting. *Geology*, 40: 875–878.

Chopin, F., Schulmann, K., Skrzypek, E., Lehmann, J., Dujardin, J. R., Martelat, J. E., Lexa, O., Corsini, M., Edel, J. B., Štípská, P. & Pitra, P., 2012. Crustal influx, indentation, ductile thinning and gravity redistribution in a continental wedge: building a Moldanubian mantled gneiss dome with underthrust Saxothuringian material (European Variscan belt). *Tectonics,* 31: TC1013.

Collett, S., Schulmann, K., Štípská, P. & Míková, J., 2020. Chronological and geochemical constraints on the Pre-Variscan tectonic history of the Erzgebirge, Saxothuringian Zone. *Gondwana Research,* 79: 27–48.

Cwojdziński, S. & Żelaźniewicz, A., 1995. Crystalline basement of the Fore-Sudetic Block. In: Cwojdziński, S. (ed.), *Geologia i ochrona środowiska bloku przedsudeckiego. Przewodnik LXVI Zjazdu Polskiego Towarzystwa Geologicznego, Annales Societatis Geologorum Poloniae, Special Volume*. Wrocław, pp. 11–28. [In Polish, with English summary.]

Cymerman, Z., Piasecki M. A. J. & Seston, R., 1997. Terranes and terrane boundaries in the Sudetes, Northeast Bohemian Massif. *Geological Magazine*, 134: 717–725.

Dall'Agnol, R., Silvabettencourt, J., Da Silvajorge-João, X., De Medeiros, H., Costi, H. & Macambira, H. B. M., 1987. Granitogenesis in northern Brazilian region: a review. *Revista Brasileira de Geociências,* 17: 382–403.

Dziedzicowa, H., 1975. Rozwój i sekwencja deformacji w strefie łupków kamieniecko-niemczańskich. In: Grocholski, A. (ed.), *Przewodnik XLVII Zjazdu Polskiego Towarzystwa Geologicznego*, *Świdnica 22–24 czerwca 1975*, Wydawnictwa Geologiczne, Warszawa, pp. 80–88. [In Polish.]

Dziedzicowa, H., 1979. Zarys budowy geologicznej wschodniego obrzeżenia gnejsów sowiogórskich. In: Gunia, T. (ed.), *Wybrane zagadnienia stratygrafii, petrografii i tektoniki wschodniego obrzeżenia gnejsów sowiogórskich i metamorfiku kłodzkiego, Materiały konferencji terenowej*. Wydawnictwa Uniwersytetu Wrocławskiego, Wrocław, pp. 43–51. [In Polish.]

Dziedzicowa, H., 1985. Variscan rejuvenation of the Precambrian gneisses along the eastern margin of the Góry Sowie massif, Fore-Sudetic Block. *Krystalinikum,* 18: 7–27.

Franke, W., Cocks, L. R. M. & Torsvik, T. H., 2017. The Palaeozoic Variscan oceans revisited. *Gondwana Research,* 48: 257–284.

Franke, W. & Żelaźniewicz, A., 2000. The eastern termination of the Variscides: terrane correlation and kinematic evolution. In: Franke, W., Haak, V., Oncken, O. & Tanner, D. (eds), *Orogenic processes: Quantification and Modelling in the Variscan Belt. Geological Society, London, Special Publications* 179, pp. 63–86.

Franke, W., Żelaźniewicz, A., Porębski, S. J. & Wajsprych, B., 1993. The Saxothuringian zone in Germany and Poland: differences and common features. *Geologische Rundschau*, 82: 583–599.

Gonçalves, G. O., Lana, C., Scholz, R., Buick, I. S., Gerdes, A., Kamo, S. L., Corfu, F., Marinhof, M. M., Chaves, A. O., Valeriano, C. & Nalini Jr., H. A., 2016. An assessment of monazite from the Itambé pegmatite district for use as U-Pb isotope reference material for microanalysis and implications for the origin of the "Moacyr" monazite. *Chemical Geology,* 424: 30–50

Gunia, T., 1979. Nowe stanowiska mikroflory w metamorfiku wschodnich okolic Niemczy. In: Gunia, T. (ed.), *Wybrane zagadnienia stratygrafii, petrografii i tektoniki wschodniego obrzeżenia gnejsów sowiogórskich i metamorfiku kłodzkiego, Materiały konferencji terenowej*. Wydawnictwa Uniwersytetu Wrocławskiego, Wrocław, pp. 63–77. [In Polish.]

Gurgurewicz, J. & Bartz, W., 2011. Deformational history of metavolcanic rocks from the Kamieniec Ząbkowicki Metamorphic Belt (Fore- Sudetic Block, southwest Poland): a quartz [c]-axis lattice preferred orientation study. *Acta Geologica Polonica,* 61: 289–305.

Hartman, J., Franks, R., Gehrels, G., Hourigan, J. & Wenig, P., 2017. Decoding dat files from a Thermo ElementTM ICP Mass Spectrometer, 15 pp. Manual available online at https://github.com/jhh67/extractdat.git [15.10.2019].

Horstwood, M. S. A., Košler, J., Gehrels, G., Jackson, S. E., McLean, N. M., Paton, Ch., Pearson, N. J., Sircombe, K., Sylvester, P., Vermeesch, P., Bowring, J. F., Condon, D. J. & Schoene, B., 2016. Community-derived standards for LA-ICP-MS U-(Th-)Pb geochronology – uncertainty propagation, age interpretation and data reporting. *Geostandards and Geoanalytical Research,* 40: 311–332.

Jackson, S. E., Pearson, N. J., Griffin, W. L. & Belousova, E. A., 2004. The application of laser ablation-inductively coupled plasma-mass spectrometry to in situ U-Pb zircon geochronology. *Chemical Geology,* 211: 47–69.

Jastrzębski, M., Budzyń, B. & Stawikowski, W., 2019. Cambro-Ordovician vs. Devono-Carboniferous geodynamic evolution of the Bohemian Massif: evidence from P-T-t studies in the Orlica-Śnieżnik Dome, SW Poland. *Geological Magazine,* 156: 447–470.

Jastrzębski, M., Żelaźniewicz, A., Murtezi, M., Larionov, A. N. & Sergeev, S., 2015. The Moldanubian Thrust Zone - a terrane boundary in the Central European Variscides refined based on lithostratigraphy and U-Pb zircon geochronology. *Lithos,* 220–223: 116–132.

Jastrzębski, M., Żelaźniewicz, A., Nowak, I., Murtezi, M. & Larionov, A. N., 2010. Protolith age and provenance of metasedimentary rocks in Variscan allochthon units: U-Pb SHRIMP zircon data from the Orlica-Śnieżnik Dome, West Sudetes. *Geological Magazine,* 147: 416–433.

Józefiak, D., 1998. The history of metamorphism of the Kamieniec Ząbkowicki mica schists (Sudetes, SW Poland). *Archiwum Mineralogiczne,* 51: 213–246. [In Polish, with English summary.]

Kennan, P. S., Dziedzic, H., Lorenc, M. W. & Mierzejewski, M. P., 1999. A review of Rb-Sr isotope patterns in the Carboniferous granitoids of the Sudetes in SW Poland. *Geologia Sudetica*, 32: 49–53.

Klimas, K., Kryza, R., Mazur, S. & Jendrzejaczyk, M., 2003. A petrogenetic comparative study of zircons from the mylonites of the Niemcza Shear Zone and the gneisses of the Góry Sowie Block (SW Poland). *Geologia Sudetica*, 35: 1–12.

Konečný, P., Kusiak, M. A. & Dunkley, D. J., 2018. Improving U-Th-Pb electron microprobe dating using monazite age references. *Chemical Geology,* 484: 22–35.

Kröner, A. & Hegner, E., 1998. Geochemistry, single zircon ages and Sm-Nd systematics of granitoid rocks from the Góry Sowie (Owl Mts, Polish West Sudetes): evidence for early Palaeozoic arc related plutonism. *Journal of the Geological Society, London*, 155: 711–724.

Kryza, R. & Fanning, C. M., 2007. Devonian deep-crustal metamorphism and exhumation in the Variscan Orogen: evidence from SHRIMP zircon ages from the HT–HP granulites and migmatites of the Góry Sowie (Polish Sudetes). *Geodinamica Acta*, 20: 159–175.

Kryza, R. & Zalasiewicz, J., 2008. Records of Precambrian–Early Palaeozoic volcanic and sedimentary processes in the Central European Variscides: A review of SHRIMP zircon data from the Kaczawa succession (Sudetes, SW Poland). *Tectonophysics,* 461: 60–71.

Kryza, R., Zalasiewicz, J., Mazur, S., Aleksandrowski, P., Sergeev, S. & Larionov, A., 2007. Precambrian crustal contribution to the Variscan accretionary prism of the Kaczawa Mountains (Sudetes, SW Poland): evidence from SHRIMP dating of detrital zircons. *International Journal of Earth Sciences,* 96: 1153–1162.

Linnemann, U., Gerdes, A., Drost, K. & Buschmann, B., 2007. The continuum between Cadomian Orogenesis and opening of the Rheic Ocean: constraints from LA-ICP-MS U-Pb zircon dating and analysis of plate-tectonic setting (Saxo-Thuringian Zone, NE Bohemian Massif, Germany). In: Linnemann, U., Nance, R. D., Kraft, P. & Zulauf, G. (eds), *The evolution of Rheic Ocean: from Avalonian-Cadomian active margin to Alleghenian-Variscan collision*. *Geological Society of America, Special Paper,* 423: 61–96.

Linnemann, U., Gerdes, A., Hofmann, M. & Marko, L., 2014. The Cadomian Orogen: neoproterozoic to Early Cambrian crustal growth and orogenic zoning along the periphery of the West African Craton-Constraints from U-Pb zircon ages and Hf isotopes (Schwarzburg Antiform, Germany). *Precambrian Research,* 244: 236–278.

Ludwig, K. R., 2012. Isoplot 3.75. A geochronological toolkit for Microsoft Excel. *Berkeley Geochronology Center Special Publication,* 5: 1–75.

Majka, J., Mazur, S., Młynarska, M., Klonowska, I., Tual, L., Kośmińska, K., Tarasiuk, J. & Wroński, S., 2019. Integrating X–ray mapping and microtomography of garnet with thermobarometry to define the P–T evolution of the (near) UHP Międzygórze eclogite, Sudetes, SW Poland. *Journal of Metamorphic Geology*, 37: 97–112.

Marheine, D., Kachlík, V., Maluski, H., Patočka, F. & Żelaźniewicz, A., 2002. The Ar-Ar ages from the West Sudetes (NE Bohemian Massif): constraints on the Variscan polyphase tectonothermal development. In: Winchester, J. A., Pharaoh, T. C. & Verniers, J. (eds), *Palaeozoic Amalgamation of Central Europe. Geological Society, London, Special Publication,* 201: 133–155.

Matte, P., Maluski, H., Rajlich, P. & Franke, W., 1990. Terrane boundaries in the Bohemian Massif: Result of large-scale Variscan shearing. *Tectonophysics,* 177: 151–170.

Mazur, S., Aleksandrowski, P., Kryza, R. & Oberc-Dziedzic, T., 2006. The Variscan Orogen in Poland. *Geological Quarterly,* 50: 89–118.

Mazur, S. & Józefiak, D., 1999. Structural record of Variscian thrusting and subsequent extensional collapse in the mica schists from vicinities of Kamieniec Ząbkowicki, Sudetic foreland, SW Poland. *Annales Societatis Geologorum Poloniae*, 69: 1–26.

Mazur, S., Kröner, A., Szczepański, J., Turniak, K., Hanžl, P., Melichar, R., Rodionov, N. V., Paderin, I. & Sergeev, S. A., 2010. Single zircon U-Pb ages and geochemistry of granitoid gneisses from SW Poland: evidence for an Avalonian affinity of the Brunian microcontinent. *Geological Magazine,* 147: 508–526.

Mazur, S. & Puziewicz, J., 1995. Mylonites of the Niemcza Fault Zone. *Annales Societatis Geologorum Poloniae*, 64: 23–52.

Mazur, S., Szczepański, J., Turniak, K. & McNaughton, N. J., 2012. Location of the Rheic suture in the eastern Bohemian Massif: Evidence from detrital zircon data. *Terra Nova* 24: 199–206.

Mazur, S., Turniak, L., Szczepański, J. & McNaughton, N. J., 2015. Vestiges of Saxothuringian crust in the Central Sudetes, Bohemian Massif: zircon evidence of a recycled subducted slab provenance. *Gondwana Research*, 27: 825–839.

Nowak, I., 1998. Polyphase exhumation of eclogite-bearing high-pressure mica schists from the Fore-Sudetic Block, SW Poland. *Geologia Sudetica*, 31: 3–31.

Oberc-Dziedzic, T., Klimas, K., Kryza, R. & Fanning, C. M., 2003. SHRIMP zircon geochronology of the Strzelin gneiss, SW Poland: evidence for a Neoproterozoic thermal event in the Fore-Sudetic Block, Central European Variscides. *International Journal of Earth Sciences*, 92: 701–711.

Oberc-Dziedzic, T., Kryza, R. & Białek, J., 2010b. Variscan multistage granitoid magmatism in Brunovistulicum: petrological and SHRIMP U/Pb zircon geochronological evidence from the southern part of the Strzelin Massif, SW Poland. *Geological Quarterly*, 54: 301–324.

Oberc-Dziedzic, T., Kryza, R., Klimas, K., Fanning, M. C. & Madej, S., 2005. Gneiss protolith ages and tectonic boundaries in the NE part of the Bohemian Massif (Fore-Sudetic Block, SW Poland). *Geological Quarterly,* 49: 363–378.

Oberc-Dziedzic, T., Kryza, R., Madej, S. & Pin, C., 2018. The Saxothuringian Terrane affinity of the metamorphic Stachów Complex (Strzelin Massif, Fore-Sudetic Block, Poland) inferred from zircon ages. *Geological Quarterly*, 62: 237–256.

Oberc-Dziedzic, T., Kryza, R., Mochnacka, K. & Larionov, A., 2010a. Ordovician passive continental margin magmatism in the Central-European Variscides: U-Pb zircon data from the SE part of the Karkonosze-Izera Massif, Sudetes, SW Poland. *International Journal of Earth Sciences*, 99: 27–46.

Oberc-Dziedzic, T., Kryza, R. & Pin, C., 2015. Variscan granitoids related to shear zones and faults: examples from the Central Sudetes (Bohemian Massif) and the Middle Odra Fault Zone. *International Journal of Earth Sciences*, 104: 1139–1166.

O'Brien, P. J., Kröner, A., Jaeckel, P., Hegener, E., Żelaźniewicz, A. & Kryza, R., 1997. Petrological and isotope studies on Palaeozoic high-pressure granulites. Góry Sowie Mts, Polish Sudetes. *Journal of Petrology,* 38: 433–456.

Oliver, G. J., Corfu, F. & Krogh, T. E., 1993. U-Pb ages from SW Poland: evidence for a Caledonian suture zone between Baltica and Gondwana. *Journal of Geological Society, London*, 150: 355–369.

Paquette, J. L. & Tiepolo, M., 2007. High resolution (5 µm) U-Th-Pb isotope dating of monazite with excimer laser ablation (ELA)-ICPMS. *Chemical Geology,* 240: 222–237.

Paulsson, O. & Andréasson, P-G., 2002. Attempted break-up of Rodinia at 850 Ma: geochronological evidence from the Seve-Kalak Superterrane, Scandinavian Caledonides. *Journal of the Geological Society, London,* 159: 751–761.

Paton, C., Woodhead, J. D., Hellstrom, J. C., Hergt, J. M., Greig, A. & Maas, R., 2010. Improved laser ablation U-Pb zircon geochronology through robust downhole fractionation correction. *Geochemistry, Geophysics, Geosystems,* 11: 1–36. Q0AA06 http://dx.doi.org/ 10.1029/2009GC002618

Petrus, J. A. & Kamber, B. S., 2012. VizualAge: A novel approach to laser ablation ICP-MS U-Pb geochronology data reduction. *Geostandards and Geoanalytical Research*, 36: 247–270.

Pietranik, A., Storey, C. & Kierczak, J., 2013. Niemcza diorites and moznodiorites (Sudetes, SW Poland): a record of changing geotectonic setting at ca. 340 Ma. *Geological Quarterly,* 57: 325–334.

Puziewicz, J., 1992. Origin of the Koźmice granodiorite (Niemcza Zone, Lower Silesia, Poland). *Archiwum Mineralogiczne,* 47: 95–146. [In Polish, with English summary.]

Rubatto, D., 2017. Zircon: The Metamorphic Mineral. *Reviews in Mineralogy and Geochemistry,* 83: 261–295.

Sawicki, L., 1965. *Mapa geologiczna regionu dolnośląskiego, 1:200 000*. Wydawnictwa Geologiczne, Warszawa. [In Polish.]

Schaltegger, U., Schmitt, A. K. & Horstwood, M. S. A., 2015 U-Th-Pb zircon geochronology by ID-TIMS, SIMS, and laser ablation ICP-MS: Recipes, interpretations, and opportunities. *Chemical Geology,* 402: 89–110.

Schneider, D. A., Zahniser, S. J., Glascock, J. M., Gordon, S. M. & Manecki, M., 2006. Thermochronology of the West Sudetes (Bohemian Massif): rapid and repeated eduction in the eastern Variscides, Poland and Czech Republic. *American Journal of Science,* 306: 846–873.

Schulmann, K., Oliot, E., Košuličová, M., Montigny, R. & Štípská, P., 2014. Variscan thermal overprints exemplified by U-Th-Pb monazite and K-Ar muscovite and biotite dating at the eastern margin of the Bohemian Massif (East Sudetes, Czech Republic). *Journal of Geosciences*, 59: 389–413.

Skrzypek, E., Bosse, V., Tetsuo Kawakami, T., Martelat, J. E. & Štípská, P., 2017. Transient allanite replacement and prograde to retrograde monazite (re)crystallization in medium-grade metasedimentary rocks from the Orlica-Śnieżnik Dome (Czech Republic/Poland): textural and geochronological arguments. *Chemical Geology*, 449: 41–57.

Sláma, J., Kosler, J., Condon, D. J., Crowley, J. L., Gerdes, A., Hanchar, J. M., Horstwood, M. S. A., Morris, G. A., Nasdala, L., Norberg, N., Schaltegger, U., Schoene, B., Tubrett, M. N. & Whitehouse, M. J., 2008. Plesovice zircon – a new natural reference material for U-Pb and Hf isotopic microanalysis. *Chemical Geology*, 249: 1–35.

Štípská, P., Chopin, F., Skrzypek, E., Schulmann, K., Pitra, P., Lexa, O., Martelat, J. E., Bollinger, C. & Žáčková, E., 2012. The juxtaposition of eclogite and mid-crustal rocks in the Orlica–Śnieżnik Dome, Bohemian Massif. *Journal of Metamorphic Geology,* 30: 213–234.

Štípská, P., Pitra, P. & Powell, R., 2006. Separate or shared metamorphic histories of eclogites and surrounding rocks? An example from the Bohemian Massif. *Journal of Metamorphic Geology*, 24: 219–240.

Szczepański, J., 2002. The $^{40}Ar/^{39}Ar$ cooling ages of white micas from Jegłowa Beds (Strzelin Massif, Fore-Sudetic Block, SW Poland). *Geologia Sudetica*, 34: 1–7.

Szczepański, J., Goleń, M. & Anczkiewicz, R., 2018. Synconvergent exhumation of volcano-sedimentary succession from the Kamieniec Metamorphic Belt (Central Sudetes, Bohemian Massif). *CETEG 2018 Abstracts, Geology, Geophysics and Environment,* 44: 196–197.

Tunheng, A. & Hirata, T., 2004. Development of signal smoothing device for precise elemental analysis using laser ablation-ICP-mass spectrometry. *Journal of Analytical Atomic Spectrometry,* 19: 932.

Tyszka, R., Kryza, R., Zalasiewicz, J. A. & Larionov, A. N., 2008. Multiple Archaean to Early Palaeozoic events of the northern Gondwana margin witnessed by detrital zircons from the Radzimowice Slates, Kaczawa Complex (Central European Variscides). *Geological Magazine*, 145: 85–93.

Van Breemen, O., Bowes, D. R., Aftalion, M. & Żelaźniewicz, A., 1988. Devonian tectonothermal activity in the Sowie Góry Gneissic Block, Sudetes, Southwestern Poland: evidence from Rb–Sr and U–Pb isotopic studies. *Annales Societatis Geologorum Poloniae,* 58: 3–19.

Walczak, K., Anczkiewicz, R., Szczepański, J., Rubatto, D. & Košler, J., 2017. Combined garnet and zircon geochronology of the ultra-high temperature metamorphism: Constraints on the rise of the Orlica-Śnieżnik Dome, NE Bohemian Massif, SW Poland. *Lithos,* 292–293: 388–400.

Wiedenbeck, M., Alle, P., Corfu, F., Griffin, W. L., Meier, M., Oberli, F., Vonquadt, A., Roddick, J. C. & Speigel, W., 1995. 3 natural zircon standards for U-Th-Pb, Lu-Hf, trace-element and REE analyses. *Geostandards Newsletter*, 19: 1–23.

Žáčková, E., Konopásek, J., Košler, J. & Jeřábek, P., 2012. Detrital zircon populations in quartzites of the Krkonoše–Jizera Massif – implications for pre-collisional history of the Saxothuringian Domain in the Bohemian Massif. *Geological Magazine,* 149: 443–458.

Žák, J. & Sláma, J., 2018. How far did the Cadomian ʽterranes' travel from Gondwana during early Palaeozoic? A critical reappraisal based on detrital zircon geochronology. *International Geology Review*, 60; 319–338.

Żelaźniewicz, A., 1995. Fore-Sudetic part of the Góry Sowie Block, SW Poland. In: Cwojdziński, S. (ed.), *Geologia i ochrona środowiska bloku przedsudeckiego. Przewodnik LXVI Zjazdu Polskiego Towarzystwa Geologicznego, Annales Societatis Geologorum Poloniae, Special Volume*. Wrocław, pp. 85–109. [In Polish, with English summary.]

Żelaźniewicz, A., Fanning, C. M. & Achramowicz, S., 2009. Refining the granite, gneiss and schist interrelationships within the Lusatian-Izera Massif, West Sudetes, using SHRIMP U-Pb zircon analyses and new geologic data. *Geologia Sudetica*, 41: 67–84.

Żelaźniewicz, A., Nowak, I., Bachliński, R., Larionov, A. N. & Sergeev, S. A., 2005. Cadomian versus younger deformations in the basement of the Moravo-Silesian Variscides, East Sudetes, SW Poland: U-Pb SHRIMP and Rb-Sr age data. *Geologia Sudetica,* 37; 35–51.

Appendix 1.

Results of the U-Pb LA-ICP-MS analyses of zircon in the mica schist SUD24/1

Analysis	Isotope ratio							Age (Ma) and discordance (%)								Concentration (ppm)			
	$^{207}Pb/^{235}U$	2σ (abs)	$^{206}Pb/^{238}U$	2σ (abs)	Rho	$^{207}Pb/^{206}Pb$	2σ (abs)	$^{207}Pb/^{235}U$	2σ (abs)	$^{206}Pb/^{238}U$	2σ (abs)	Disc.[1] §	$^{207}Pb/^{206}Pb$	2σ (abs)	Disc.[2] §	Th	U	Pb	Th/U
1	6.410	0.350	0.353	0.019	0.78	0.1296	0.0051	2018	49	1939	90	3.9	2068	70	6.2	158	319	472	0.5
3	6.060	0.310	0.339	0.014	0.71	0.1270	0.0045	1980	45	1879	66	5.1	2049	64	8.3	111	343	319	0.3
4*	0.750	0.017	0.092	0.002	0.61	0.0594	0.0010	567	10	564	11	0.5	578	33	2.4	632	783	509	0.8
6	0.854	0.022	0.101	0.002	0.54	0.0620	0.0012	625	12	620	13	0.8	656	40	5.5	353	399	351	0.9
8	0.916	0.025	0.109	0.003	0.59	0.0608	0.0013	657	13	666	16	-1.4	608	46	-9.5	136	287	147	0.5
9	0.744	0.022	0.089	0.003	0.52	0.0609	0.0014	565	13	547	15	3.2	615	49	11.1	512	2001	492	0.3
11	0.772	0.019	0.093	0.002	0.60	0.0602	0.0011	581	11	577	13	0.7	594	40	2.9	459	728	427	0.6
12	0.947	0.024	0.112	0.003	0.50	0.0616	0.0013	676	12	686	15	-1.4	634	44	-8.2	310	422	365	0.7
14	0.787	0.019	0.096	0.002	0.53	0.0595	0.0010	590	11	588	12	0.3	573	39	-2.6	466	644	437	0.7
17	3.118	0.081	0.250	0.006	0.36	0.0899	0.0024	1435	20	1439	32	-0.3	1418	48	-1.5	51	139	97	0.4
19	8.190	0.260	0.399	0.014	0.40	0.1495	0.0047	2250	29	2160	63	4.0	2330	54	7.3	12	546	30	0.0
20	0.787	0.021	0.094	0.003	0.47	0.0613	0.0014	588	12	579	15	1.5	623	49	7.1	493	1009	409	0.5
21	6.710	0.280	0.369	0.016	0.68	0.1315	0.0042	2071	37	2024	74	2.3	2112	57	4.2	97	153	253	0.6
23*	0.741	0.019	0.091	0.002	0.67	0.0593	0.0010	562	11	558	12	0.7	572	36	2.4	439	745	312	0.6
24	1.693	0.055	0.168	0.005	0.60	0.0730	0.0018	1001	20	999	25	0.2	973	52	-2.7	58	76	82	0.8
26	5.270	0.180	0.325	0.011	0.58	0.1181	0.0033	1856	28	1814	55	2.3	1923	48	5.7	72	101	215	0.7
27*	0.723	0.019	0.089	0.002	0.61	0.0594	0.0013	550	11	547	12	0.6	550	45	0.5	269	622	218	0.4
29	0.819	0.022	0.098	0.003	0.58	0.0612	0.0013	606	12	599	15	1.1	622	45	3.7	219	456	189	0.5
30	0.814	0.022	0.098	0.003	0.63	0.0604	0.0013	602	12	603	15	-0.2	588	46	-2.6	131	344	130	0.4
31	0.983	0.031	0.114	0.003	0.54	0.0626	0.0016	690	16	696	19	-0.9	657	54	-5.9	169	135	187	1.3
32	0.888	0.027	0.105	0.003	0.62	0.0612	0.0014	643	14	645	17	-0.3	620	47	-4.0	191	313	205	0.6
35	24.880	0.700	0.652	0.019	0.79	0.2760	0.0049	3301	27	3233	74	2.1	3337	28	3.1	330	246	1388	1.3
37	0.823	0.021	0.100	0.002	0.59	0.0599	0.0011	609	12	614	13	-0.9	581	41	-5.7	39	380	34	0.1
39	0.803	0.023	0.096	0.003	0.68	0.0609	0.0012	599	13	592	15	1.2	611	44	3.1	257	226	203	1.1

Analysis	Isotope ratio							Age (Ma) and discordance (%)								Concentration (ppm)			
	$^{207}Pb/^{235}U$	2σ (abs)	$^{206}Pb/^{238}U$	2σ (abs)	Rho	$^{207}Pb/^{206}Pb$	2σ (abs)	$^{207}Pb/^{235}U$	2σ (abs)	$^{206}Pb/^{238}U$	2σ (abs)	Disc.[1] §	$^{207}Pb/^{206}Pb$	2σ (abs)	Disc.[2] §	Th	U	Pb	Th/U
40	0.879	0.023	0.096	0.002	0.59	0.0671	0.0013	637	12	589	13	7.6	824	41	28.5	327	397	275	0.8
41	6.470	0.330	0.361	0.018	0.94	0.1294	0.0024	2035	44	1982	82	2.6	2087	32	5.0	89	138	232	0.6
42	0.790	0.022	0.095	0.002	0.65	0.0602	0.0011	590	12	585	14	0.8	596	43	1.8	288	435	225	0.7
43	0.919	0.033	0.108	0.003	0.45	0.0617	0.0019	659	17	660	15	-0.2	628	64	-5.1	312	123	262	2.5
44	0.904	0.028	0.108	0.003	0.61	0.0611	0.0014	651	14	660	15	-1.4	613	49	-7.7	410	208	348	2.0
45	1.719	0.053	0.172	0.004	0.58	0.0725	0.0017	1014	19	1026	25	-1.2	985	49	-4.2	110	174	152	0.6
46	0.772	0.018	0.094	0.002	0.62	0.0603	0.0011	581	10	578	12	0.6	597	38	3.2	664	1138	547	0.6
47	0.889	0.023	0.105	0.003	0.57	0.0614	0.0012	643	12	644	14	-0.1	626	43	-2.9	178	367	162	0.5
48	0.902	0.028	0.105	0.003	0.58	0.0623	0.0013	649	15	642	17	1.1	666	48	3.6	236	313	232	0.8
51	0.854	0.029	0.099	0.003	0.73	0.0623	0.0013	623	17	605	19	2.9	666	48	9.2	138	211	145	0.7
52	0.806	0.019	0.096	0.002	0.52	0.0602	0.0011	598	11	592	14	1.0	592	41	0.0	244	467	258	0.5
53	11.950	0.420	0.491	0.019	0.74	0.1763	0.0040	2596	33	2564	83	1.2	2608	38	1.7	180	203	851	0.9
54	0.885	0.026	0.104	0.003	0.62	0.0618	0.0014	641	15	636	17	0.8	648	48	1.9	286	301	316	1.0
55	0.812	0.020	0.090	0.002	0.56	0.0652	0.0013	602	11	557	13	7.5	776	42	28.2	420	790	449	0.5
57	0.874	0.030	0.104	0.003	0.61	0.0608	0.0016	633	16	638	18	-0.8	586	56	-8.9	34	205	29	0.2
58	6.880	0.190	0.378	0.010	0.64	0.1316	0.0025	2095	23	2070	45	1.2	2108	34	1.8	125	183	334	0.7
59	4.490	0.130	0.292	0.009	0.60	0.1119	0.0026	1720	24	1657	44	3.7	1808	42	8.4	74	143	165	0.5
60	1.267	0.032	0.137	0.003	0.59	0.0668	0.0012	828	14	825	19	0.4	821	39	-0.5	830	670	825	1.2
61	1.055	0.033	0.119	0.004	0.54	0.0653	0.0017	726	16	722	21	0.6	745	56	3.1	43	118	37	0.4
62	0.693	0.021	0.081	0.003	0.59	0.0631	0.0018	532	12	504	15	5.3	653	49	22.8	1974	1687	1321	1.2
63	0.732	0.019	0.084	0.002	0.52	0.0640	0.0014	557	11	521	13	6.5	706	46	26.2	806	1161	564	0.7
64	1.250	0.040	0.123	0.004	0.66	0.0741	0.0017	822	18	747	20	9.1	1009	49	26.0	93	167	102	0.6
65	0.925	0.028	0.098	0.003	0.53	0.0689	0.0017	661	15	604	16	8.6	867	51	30.3	264	320	249	0.8
66	1.872	0.072	0.181	0.007	0.71	0.0751	0.0020	1070	25	1065	37	0.5	1050	55	-1.4	121	156	182	0.8
67	0.875	0.022	0.101	0.003	0.45	0.0628	0.0014	637	12	619	15	2.8	691	48	10.4	194	427	179	0.5
68	0.803	0.023	0.096	0.002	0.56	0.0609	0.0014	596	13	588	13	1.3	612	47	3.9	356	181	281	2.0

70	0.804	0.023	0.096	0.003	0.68	0.0608	0.0013	598	13	593	16	0.8	612	44	3.1	490	619	434	0.8
72*	0.742	0.019	0.090	0.002	0.55	0.0599	0.0012	562	11	553	12	1.5	575	44	3.8	292	528	246	0.6
73	6.840	0.200	0.387	0.011	0.76	0.1295	0.0025	2080	26	2111	55	-1.5	2069	34	-2.0	300	243	1024	1.2
76	0.881	0.032	0.103	0.003	0.51	0.0622	0.0019	642	16	630	18	1.9	671	62	6.1	369	205	309	1.8
77	0.927	0.037	0.109	0.003	0.56	0.0619	0.0020	657	19	664	19	-1.1	602	70	-10.3	51	37	48	1.4
78	1.172	0.032	0.129	0.003	0.63	0.0665	0.0014	783	15	778	19	0.6	803	45	3.1	239	290	276	0.8
80	0.824	0.033	0.098	0.004	0.68	0.0618	0.0018	608	18	598	21	1.6	617	63	3.1	525	239	461	2.2
81	0.793	0.027	0.097	0.003	0.57	0.0604	0.0016	594	15	594	18	0.0	565	56	-5.1	229	124	196	1.8
82	0.989	0.052	0.108	0.005	0.47	0.0673	0.0029	691	27	660	27	4.5	771	93	14.4	118	88	118	1.3
84	1.094	0.037	0.124	0.003	0.49	0.0636	0.0018	746	18	754	18	-1.1	688	60	-9.6	38	49	42	0.8
85*	0.748	0.031	0.092	0.003	0.39	0.0588	0.0022	566	18	570	17	-0.7	530	85	-7.5	78	80	69	1.0
86	0.926	0.024	0.110	0.003	0.60	0.0615	0.0012	665	13	673	16	-1.2	638	43	-5.5	1248	561	1164	2.2
87	0.869	0.027	0.104	0.003	0.73	0.0611	0.0013	633	15	634	18	-0.2	610	47	-3.9	199	226	210	0.9
91	0.809	0.023	0.097	0.003	0.60	0.0606	0.0013	599	13	596	15	0.5	599	48	0.5	435	408	428	1.1
93	0.939	0.031	0.112	0.004	0.61	0.0613	0.0016	668	16	679	21	-1.6	610	56	-11.3	98	118	109	0.8
94	7.470	0.220	0.399	0.011	0.73	0.1350	0.0025	2168	25	2161	51	0.3	2157	33	-0.2	133	225	477	0.6
95	0.871	0.029	0.105	0.003	0.60	0.0611	0.0015	632	15	643	18	-1.7	604	56	-6.5	200	134	203	1.5
97	0.824	0.026	0.095	0.003	0.48	0.0640	0.0019	607	14	583	19	4.0	689	63	15.4	622	634	579	1.0
99	1.366	0.048	0.133	0.004	0.53	0.0750	0.0022	868	21	807	23	7.0	1033	59	21.9	35	73	52	0.5
100	0.777	0.022	0.094	0.003	0.55	0.0598	0.0014	580	13	578	15	0.3	570	50	-1.4	157	414	137	0.4
105	0.855	0.022	0.101	0.002	0.63	0.0617	0.0012	625	12	619	14	1.0	647	39	4.3	403	591	346	0.7
107	0.789	0.026	0.096	0.003	0.55	0.0607	0.0016	588	16	591	19	-0.5	594	57	0.5	204	159	161	1.3
108	6.500	0.190	0.365	0.009	0.77	0.1287	0.0023	2037	25	2002	42	1.7	2072	32	3.4	377	296	1000	1.3
110	0.966	0.036	0.108	0.004	0.70	0.0650	0.0018	684	19	662	26	3.2	754	57	12.2	448	380	421	1.2
111	5.920	0.210	0.341	0.010	0.44	0.1284	0.0040	1959	32	1887	49	3.7	2050	50	8.0	91	88	272	1.0
112	0.825	0.026	0.098	0.003	0.48	0.0615	0.0015	607	15	600	17	1.2	630	56	4.8	309	615	263	0.5
113	0.921	0.029	0.110	0.003	0.62	0.0608	0.0013	658	15	670	18	-1.8	604	50	-10.9	159	198	169	0.8
114	0.935	0.029	0.111	0.003	0.61	0.0615	0.0014	672	15	676	18	-0.6	622	49	-8.7	132	154	137	0.9
115	4.820	0.150	0.316	0.009	0.58	0.1117	0.0027	1778	27	1761	44	1.0	1811	43	2.8	44	71	140	0.6

Analysis	Isotope ratio							Age (Ma) and discordance (%)								Concentration (ppm)			
	$^{207}Pb/^{235}U$	2σ (abs)	$^{206}Pb/^{238}U$	2σ (abs)	Rho	$^{207}Pb/^{206}Pb$	2σ (abs)	$^{207}Pb/^{235}U$	2σ (abs)	$^{206}Pb/^{238}U$	2σ (abs)	Disc.[1] §	$^{207}Pb/^{206}Pb$	2σ (abs)	Disc.[2] §	Th	U	Pb	Th/U
117	5.630	0.170	0.344	0.009	0.62	0.1186	0.0026	1918	26	1904	44	0.7	1927	40	1.2	383	736	1223	0.5
118	0.816	0.026	0.100	0.003	0.74	0.0600	0.0014	605	16	612	18	-1.2	576	50	-6.3	67	158	72	0.4
120	0.892	0.031	0.106	0.003	0.49	0.0618	0.0019	641	16	647	18	-0.9	609	64	-6.2	57	80	67	0.7
121	5.340	0.170	0.330	0.010	0.73	0.1178	0.0025	1873	28	1834	50	2.1	1916	40	4.3	90	277	298	0.3
123	1.836	0.059	0.175	0.005	0.66	0.0763	0.0017	1056	22	1037	28	1.8	1089	46	4.8	112	193	233	0.6
124	0.808	0.028	0.097	0.003	0.63	0.0610	0.0016	598	16	593	18	0.8	603	54	1.7	299	332	315	0.9
125	0.847	0.022	0.097	0.003	0.52	0.0635	0.0014	622	12	597	15	4.0	708	47	15.7	908	1568	666	0.6
126	0.844	0.029	0.102	0.003	0.62	0.0608	0.0018	617	16	622	19	-0.8	588	63	-5.8	25	91	29	0.3
128	0.819	0.030	0.094	0.003	0.60	0.0634	0.0018	607	17	579	19	4.6	691	59	16.2	596	333	441	1.8
129	0.936	0.029	0.107	0.003	0.59	0.0641	0.0016	668	15	651	18	2.5	722	51	9.8	911	535	684	1.7
130	0.852	0.030	0.101	0.003	0.73	0.0605	0.0013	620	16	619	18	0.2	594	45	-4.2	243	251	160	1.0
131	0.894	0.022	0.103	0.002	0.56	0.0625	0.0011	647	12	633	12	2.2	683	38	7.3	1280	1016	721	1.3
133	5.970	0.190	0.358	0.009	0.35	0.1210	0.0036	1960	28	1970	42	-0.5	1939	54	-1.6	49	18	105	2.7
134	0.793	0.025	0.097	0.003	0.65	0.0596	0.0013	590	14	594	16	-0.7	577	48	-2.9	149	174	90	0.9
135	0.835	0.027	0.100	0.003	0.53	0.0607	0.0016	615	15	615	17	0.0	581	56	-5.9	132	129	85	1.0
136	0.813	0.025	0.096	0.003	0.72	0.0611	0.0012	602	14	594	16	1.3	620	44	4.2	198	287	117	0.7
137	1.459	0.044	0.151	0.004	0.54	0.0703	0.0017	911	18	904	23	0.8	927	48	2.5	216	282	218	0.8
138	0.827	0.025	0.101	0.003	0.68	0.0596	0.0013	609	14	621	16	-2.0	566	48	-9.7	466	219	319	2.1
139	1.453	0.035	0.149	0.003	0.55	0.0707	0.0013	909	15	895	19	1.5	941	38	4.9	168	797	184	0.2
Rejected data (disc. >10%)																			
~~2~~	~~0.924~~	~~0.027~~	~~0.094~~	~~0.003~~	~~0.59~~	~~0.0718~~	~~0.0015~~	~~663~~	~~14~~	~~580~~	~~15~~	~~12.5~~	~~973~~	~~44~~	~~40.4~~	~~572~~	~~738~~	~~585~~	~~0.8~~
~~5~~	~~5.370~~	~~0.140~~	~~0.317~~	~~0.008~~	~~0.61~~	~~0.1223~~	~~0.0023~~	~~1877~~	~~22~~	~~1774~~	~~39~~	~~5.5~~	~~1983~~	~~33~~	~~10.5~~	~~247~~	~~811~~	~~699~~	~~0.3~~
~~7~~	~~2.276~~	~~0.069~~	~~0.176~~	~~0.005~~	~~0.60~~	~~0.0943~~	~~0.0023~~	~~1199~~	~~22~~	~~1041~~	~~28~~	~~13.2~~	~~1492~~	~~46~~	~~30.2~~	~~56~~	~~158~~	~~124~~	~~0.4~~
~~10~~	~~2.281~~	~~0.097~~	~~0.195~~	~~0.008~~	~~0.76~~	~~0.0853~~	~~0.0022~~	~~1190~~	~~31~~	~~1139~~	~~41~~	~~4.3~~	~~1283~~	~~51~~	~~11.2~~	~~14~~	~~107~~	~~36~~	~~0.1~~
~~13~~	~~10.210~~	~~0.250~~	~~0.405~~	~~0.010~~	~~0.62~~	~~0.1819~~	~~0.0030~~	~~2449~~	~~22~~	~~2186~~	~~43~~	~~10.7~~	~~2663~~	~~27~~	~~17.9~~	~~184~~	~~356~~	~~776~~	~~0.5~~

15	4.169	0.096	0.270	0.006	0.63	0.1113	0.0018	1665	19	1543	30	7.3	1816	28	15.0	226	439	489	0.5
16	0.974	0.035	0.093	0.003	0.67	0.0767	0.0019	688	18	569	16	17.3	1089	52	47.8	239	456	275	0.5
18	2.180	0.087	0.113	0.003	0.48	0.1405	0.0044	1160	28	686	18	40.9	2165	61	68.3	40	101	104	0.4
22	7.990	0.210	0.366	0.009	0.54	0.1591	0.0037	2228	25	2007	44	9.9	2439	40	17.7	266	492	851	0.5
25	2.500	0.085	0.135	0.006	0.27	0.1395	0.0089	1263	25	814	33	35.6	2132	75	61.8	116	1594	338	0.1
28	4.130	0.160	0.266	0.011	0.62	0.1129	0.0039	1649	33	1516	53	8.1	1822	63	16.8	113	373	345	0.3
33	2.074	0.083	0.096	0.004	0.57	0.1595	0.0049	1132	28	593	24	47.6	2400	58	75.3	118	217	265	0.5
34	6.110	0.260	0.315	0.014	0.62	0.1430	0.0052	1983	36	1755	69	11.5	2239	63	21.6	60	88	204	0.7
36	4.390	0.150	0.246	0.008	0.65	0.1300	0.0031	1696	28	1413	41	16.7	2071	41	31.8	266	337	881	0.8
38	2.810	0.110	0.186	0.008	0.61	0.1108	0.0036	1355	29	1102	43	18.7	1792	59	38.5	90	247	271	0.4
49	4.210	0.120	0.214	0.006	0.56	0.1440	0.0033	1674	24	1243	34	25.7	2258	41	45.0	73	220	382	0.3
50	1.797	0.061	0.168	0.006	0.62	0.0771	0.0020	1040	22	1000	31	3.8	1112	51	10.1	464	586	859	0.8
56	0.834	0.024	0.083	0.002	0.61	0.0733	0.0016	612	13	515	13	15.8	986	44	47.8	977	1193	892	0.8
69	2.180	0.069	0.180	0.005	0.67	0.0879	0.0020	1168	22	1067	28	8.6	1365	41	21.8	75	265	152	0.3
71	6.260	0.160	0.333	0.007	0.61	0.1357	0.0024	2011	22	1851	35	8.0	2163	30	14.4	211	428	648	0.5
74	0.910	0.030	0.095	0.003	0.49	0.0698	0.0023	654	16	585	20	10.6	885	64	33.9	1510	1434	1384	1.1
75	1.466	0.055	0.093	0.003	0.36	0.1154	0.0038	903	23	570	16	36.9	1821	65	68.7	56	113	83	0.5
79	3.770	0.130	0.250	0.008	0.71	0.1101	0.0024	1574	28	1431	43	9.1	1795	39	20.3	43	244	109	0.2
83	1.046	0.043	0.096	0.003	0.33	0.0801	0.0033	723	21	590	18	18.4	1128	83	47.7	60	43	55	1.4
88	4.095	0.110	0.228	0.006	0.50	0.1316	0.0034	1647	21	1325	32	19.6	2079	36	36.3	130	501	499	0.3
89	2.225	0.098	0.152	0.007	0.72	0.1067	0.0035	1178	31	910	38	22.8	1711	60	46.8	56	230	207	0.2
90	1.053	0.060	0.092	0.004	0.35	0.0847	0.0045	719	31	566	26	21.3	1190	110	52.4	98	181	137	0.5
92	0.912	0.026	0.094	0.003	0.65	0.0707	0.0017	656	14	578	15	11.9	925	47	37.5	466	614	488	0.8
96	1.261	0.068	0.065	0.003	0.76	0.1407	0.0049	813	30	402	20	50.6	2188	66	81.6	58	333	183	0.2
98	1.489	0.074	0.122	0.006	0.75	0.0906	0.0027	913	30	735	32	19.5	1394	60	47.3	27	176	71	0.2
101	1.048	0.032	0.093	0.003	0.46	0.0814	0.0021	723	16	574	16	20.6	1210	52	52.6	148	383	191	0.4
102	1.024	0.032	0.087	0.002	0.52	0.0860	0.0023	713	16	536	15	24.8	1306	51	59.0	328	708	401	0.5
103	1.308	0.044	0.117	0.004	0.51	0.0818	0.0024	846	20	712	21	15.8	1206	56	41.0	131	212	173	0.6
104	1.840	0.063	0.076	0.002	0.44	0.1773	0.0056	1049	23	474	14	54.8	2583	55	81.6	121	830	691	0.1

Analysis	Isotope ratio							Age (Ma) and discordance (%)								Concentration (ppm)			
	$^{207}Pb/^{235}U$	2σ (abs)	$^{206}Pb/^{238}U$	2σ (abs)	Rho	$^{207}Pb/^{206}Pb$	2σ (abs)	$^{207}Pb/^{235}U$	2σ (abs)	$^{206}Pb/^{238}U$	2σ (abs)	Disc.[1] §	$^{207}Pb/^{206}Pb$	2σ (abs)	Disc.[2] §	Th	U	Pb	Th/U
~~106~~	~~1.271~~	~~0.040~~	~~0.113~~	~~0.003~~	~~0.57~~	~~0.0816~~	~~0.0021~~	~~830~~	~~17~~	~~690~~	~~19~~	~~16.9~~	~~1204~~	~~49~~	~~42.7~~	~~298~~	~~831~~	~~479~~	~~0.4~~
~~109~~	~~5.570~~	~~0.190~~	~~0.270~~	~~0.011~~	~~0.58~~	~~0.1536~~	~~0.0062~~	~~1893~~	~~29~~	~~1527~~	~~56~~	~~19.3~~	~~2321~~	~~55~~	~~34.2~~	~~504~~	~~629~~	~~1707~~	~~0.8~~
~~116~~	~~4.730~~	~~0.170~~	~~0.298~~	~~0.011~~	~~0.72~~	~~0.1167~~	~~0.0029~~	~~1765~~	~~33~~	~~1677~~	~~56~~	~~5.0~~	~~1894~~	~~46~~	~~11.5~~	~~117~~	~~158~~	~~402~~	~~0.7~~
~~119~~	~~10.790~~	~~0.410~~	~~0.388~~	~~0.015~~	~~0.75~~	~~0.2025~~	~~0.0054~~	~~2497~~	~~36~~	~~2108~~	~~68~~	~~15.6~~	~~2838~~	~~44~~	~~25.7~~	~~72~~	~~253~~	~~299~~	~~0.3~~
~~122~~	~~3.447~~	~~0.110~~	~~0.236~~	~~0.007~~	~~0.77~~	~~0.1067~~	~~0.0021~~	~~1505~~	~~27~~	~~1362~~	~~37~~	~~9.5~~	~~1725~~	~~37~~	~~21.0~~	~~54~~	~~169~~	~~194~~	~~0.3~~
~~127~~	~~0.959~~	~~0.039~~	~~0.098~~	~~0.004~~	~~0.71~~	~~0.0709~~	~~0.0019~~	~~676~~	~~21~~	~~604~~	~~23~~	~~10.7~~	~~934~~	~~56~~	~~35.3~~	~~131~~	~~248~~	~~121~~	~~0.5~~
~~132~~	~~5.770~~	~~0.150~~	~~0.321~~	~~0.008~~	~~0.75~~	~~0.1299~~	~~0.0023~~	~~1939~~	~~23~~	~~1790~~	~~39~~	~~7.7~~	~~2087~~	~~31~~	~~14.2~~	~~191~~	~~402~~	~~345~~	~~0.5~~
~~140~~	~~0.911~~	~~0.048~~	~~0.093~~	~~0.005~~	~~0.73~~	~~0.0728~~	~~0.0027~~	~~651~~	~~27~~	~~573~~	~~29~~	~~12.0~~	~~945~~	~~80~~	~~39.4~~	~~446~~	~~301~~	~~363~~	~~1.5~~

Comments: * – analysis used for calculations of maximum depositional age; § disc.[1] = $\{1 - [(^{206}Pb/^{238}U) / (^{207}Pb/^{235}U)]\} \times 100$ for zircon younger than 1 Ga; disc.[2] = $\{1 - [(^{206}Pb/^{238}U) / (^{207}Pb/^{206}Pb)]\} \times 100$ for zircon older than 1 Ga.

Appendix 2.

The EPMA results presenting composition of the monazite in the mica schist samples SUD24/1 and SUD24/2

Analysis	P_2O_5	As_2O_5	SiO_2	ThO_2	UO_2	Al_2O_3	Y_2O_3	La_2O_3	Ce_2O_3	Pr_2O_3	Nd_2O_3	Sm_2O_3	Eu_2O_3	Gd_2O_3	Tb_2O_3	Dy_2O_3	Ho_2O_3	Er_2O_3	Tm_2O_3	Yb_2O_3	Lu_2O_3	CaO	FeO	SrO	PbO	K_2O	SO_3	Total
SUD24/1																												
mnz1-1	30.51	b.d.l.	0.40	7.34	0.82	b.d.l.	2.21	12.41	24.40	2.84	10.26	2.00	0.35	1.68	0.21	0.80	b.d.l.	0.41	b.d.l.	0.16	b.d.l.	1.60	0.95	b.d.l.	0.12	b.d.l.	b.d.l.	99.48
mnz1-2	29.63	b.d.l.	0.36	6.75	0.78	0.25	2.22	13.19	24.97	2.80	9.78	1.93	0.36	1.47	0.17	0.73	b.d.l.	0.41	b.d.l.	0.12	b.d.l.	1.55	0.92	0.04	0.12	b.d.l.	b.d.l.	98.55
mnz2-1	30.70	b.d.l.	0.49	2.79	0.58	b.d.l.	0.47	15.35	29.78	3.41	12.08	2.00	b.d.l.	1.03	b.d.l.	b.d.l.	b.d.l.	0.29	0.10	0.18	b.d.l.	0.36	0.32	b.d.l.	0.07	0.04	0.02	100.06
mnz3-1	29.98	b.d.l.	0.83	4.64	0.24	b.d.l.	0.59	15.00	29.13	3.32	12.02	2.00	b.d.l.	1.10	b.d.l.	b.d.l.	b.d.l.	0.42	b.d.l.	0.18	b.d.l.	0.33	b.d.l.	b.d.l.	0.07	b.d.l.	b.d.l.	99.84
mnz4-1	30.32	b.d.l.	0.21	4.71	0.90	b.d.l.	1.00	14.01	27.87	3.22	11.67	2.07	0.26	1.18	b.d.l.	0.23	b.d.l.	0.39	b.d.l.	0.12	b.d.l.	1.18	0.16	b.d.l.	0.10	b.d.l.	b.d.l.	99.60
mnz5-1	30.78	b.d.l.	0.17	3.91	0.30	b.d.l.	0.97	16.25	29.53	3.18	9.94	1.40	0.23	0.70	b.d.l.	0.27	b.d.l.	0.42	b.d.l.	0.13	b.d.l.	0.85	0.78	b.d.l.	0.06	0.01	b.d.l.	99.88
mnz5-2	30.80	b.d.l.	0.15	3.20	0.36	b.d.l.	1.24	16.20	29.50	3.07	10.11	1.50	0.23	0.81	b.d.l.	0.43	b.d.l.	0.50	0.10	0.21	b.d.l.	0.71	0.83	0.04	0.06	0.01	b.d.l.	100.07
mnz7-1	30.26	b.d.l.	0.74	4.01	0.67	b.d.l.	1.47	11.60	28.00	3.55	13.10	2.34	b.d.l.	1.83	0.21	0.63	b.d.l.	0.41	b.d.l.	0.15	b.d.l.	0.56	0.43	b.d.l.	0.07	b.d.l.	b.d.l.	100.04
mnz8-1	30.47	b.d.l.	0.53	3.15	0.93	b.d.l.	1.67	13.37	27.79	3.29	11.98	2.19	0.21	1.55	0.17	0.54	b.d.l.	0.45	0.13	0.16	b.d.l.	0.56	0.52	b.d.l.	0.08	b.d.l.	b.d.l.	99.73
mnz8-2	30.45	b.d.l.	0.53	3.77	0.81	b.d.l.	1.53	13.68	27.78	3.28	11.75	2.07	0.19	1.46	0.13	0.57	b.d.l.	0.36	b.d.l.	0.16	b.d.l.	0.58	0.52	b.d.l.	0.09	b.d.l.	0.03	99.73
mnz8-3	30.43	b.d.l.	0.47	2.48	0.88	b.d.l.	1.98	13.12	27.52	3.34	12.30	2.23	b.d.l.	1.84	0.19	0.77	b.d.l.	0.43	0.10	0.18	b.d.l.	0.58	0.99	b.d.l.	0.07	0.01	b.d.l.	99.93
mnz8-4	30.21	b.d.l.	0.64	4.09	0.38	b.d.l.	1.49	14.03	27.94	3.32	12.03	2.11	b.d.l.	1.59	0.16	0.57	b.d.l.	0.37	b.d.l.	0.10	b.d.l.	0.51	0.48	b.d.l.	0.07	b.d.l.	0.02	100.14
mnz9-2	31.14	b.d.l.	0.28	4.32	0.66	b.d.l.	0.17	14.99	29.28	3.36	11.41	1.94	0.29	1.09	0.09	b.d.l.	b.d.l.	0.27	0.12	0.14	b.d.l.	0.90	0.16	0.09	0.09	0.05	0.02	100.87
mnz9-2	30.42	b.d.l.	0.29	4.45	0.47	b.d.l.	0.03	14.76	28.72	3.31	12.11	2.04	0.29	1.00	b.d.l.	b.d.l.	b.d.l.	0.36	0.09	0.11	b.d.l.	0.91	0.10	0.10	0.08	0.02	0.03	99.70
mnz9-3	30.89	b.d.l.	0.26	4.37	0.66	b.d.l.	0.15	14.72	28.91	3.28	11.66	2.07	0.27	1.18	0.09	b.d.l.	b.d.l.	0.28	b.d.l.	0.10	b.d.l.	0.87	0.10	0.11	0.09	0.02	b.d.l.	100.10
mnz10-1	29.78	b.d.l.	0.86	7.82	0.90	b.d.l.	0.69	13.57	28.16	3.17	10.35	1.69	0.18	0.87	b.d.l.	b.d.l.	b.d.l.	0.42	b.d.l.	0.16	b.d.l.	1.11	0.44	0.05	0.14	0.05	b.d.l.	100.40
mnz11-1	30.05	b.d.l.	0.96	7.10	0.47	b.d.l.	0.53	14.21	27.61	3.18	11.44	2.01	b.d.l.	1.10	b.d.l.	0.18	b.d.l.	0.45	b.d.l.	0.11	b.d.l.	0.77	0.19	b.d.l.	0.11	0.05	b.d.l.	100.53
mnz12-1	30.36	b.d.l.	0.55	4.27	0.51	b.d.l.	0.40	15.04	30.09	3.41	11.36	1.93	b.d.l.	1.02	b.d.l.	0.18	b.d.l.	0.38	0.10	0.15	b.d.l.	0.56	0.14	b.d.l.	0.08	0.02	0.03	100.58
mnz13-1	30.34	b.d.l.	0.30	4.46	0.55	b.d.l.	0.30	12.33	28.14	3.47	13.05	2.52	0.38	1.62	0.09	0.22	b.d.l.	0.39	b.d.l.	0.14	b.d.l.	0.88	0.28	0.09	0.09	b.d.l.	b.d.l.	99.64
mnz13-2	30.40	b.d.l.	0.28	4.20	0.59	b.d.l.	0.38	14.05	28.42	3.25	11.79	2.04	0.36	1.33	b.d.l.	0.26	b.d.l.	0.27	0.12	0.12	b.d.l.	0.84	0.39	0.09	0.09	b.d.l.	b.d.l.	99.26
mnz14-1	30.77	b.d.l.	0.20	3.20	0.79	b.d.l.	0.80	14.35	28.51	3.31	11.97	2.21	0.33	1.33	b.d.l.	0.31	b.d.l.	0.42	0.10	0.18	b.d.l.	0.75	0.20	b.d.l.	0.08	0.05	b.d.l.	99.86
mnz15-2	30.56	b.d.l.	0.29	1.58	0.87	b.d.l.	0.93	14.66	29.28	3.42	12.40	2.24	0.23	1.38	b.d.l.	0.31	b.d.l.	0.28	b.d.l.	0.17	b.d.l.	0.41	0.09	b.d.l.	0.06	0.01	b.d.l.	99.16
mnz16-1	29.46	b.d.l.	1.01	4.37	0.97	b.d.l.	0.89	14.14	28.42	3.33	11.97	2.13	0.17	1.24	b.d.l.	0.33	b.d.l.	0.36	b.d.l.	0.15	b.d.l.	0.44	0.19	b.d.l.	0.11	0.05	b.d.l.	99.73
mnz17-1	28.88	b.d.l.	1.39	6.91	0.70	b.d.l.	1.81	12.34	26.92	3.19	11.68	2.13	0.19	1.62	0.13	0.71	b.d.l.	0.48	0.12	0.23	b.d.l.	0.48	0.23	b.d.l.	0.12	b.d.l.	0.03	100.30
mnz17-2	29.25	b.d.l.	1.08	6.16	0.73	b.d.l.	1.91	13.42	27.26	3.26	11.14	1.85	0.26	1.32	0.10	0.61	b.d.l.	0.52	0.09	0.21	b.d.l.	0.58	0.32	b.d.l.	0.11	0.01	b.d.l.	100.20
mnz18-1	30.15	b.d.l.	0.31	4.66	0.59	b.d.l.	0.06	15.31	28.53	3.26	11.75	1.92	0.24	0.93	b.d.l.	b.d.l.	b.d.l.	0.38	b.d.l.	0.15	b.d.l.	0.95	b.d.l.	0.11	0.10	b.d.l.	0.03	99.41
mnz18-2	30.06	b.d.l.	0.34	4.80	0.50	b.d.l.	0.35	14.86	28.21	3.26	11.99	2.00	0.28	1.15	0.09	b.d.l.	b.d.l.	0.35	0.09	0.15	b.d.l.	0.90	b.d.l.	0.12	0.09	b.d.l.	0.02	99.60
mnz18-3	30.32	b.d.l.	0.23	3.69	0.74	b.d.l.	0.07	14.54	28.76	3.37	12.34	2.21	0.33	1.11	b.d.l.	b.d.l.	b.d.l.	0.29	0.09	0.12	b.d.l.	0.80	0.09	0.08	0.08	0.01	b.d.l.	99.29

Analysis	P_2O_5	As_2O_5	SiO_2	ThO_2	UO_2	Al_2O_3	Y_2O_3	La_2O_3	Ce_2O_3	Pr_2O_3	Nd_2O_3	Sm_2O_3	Eu_2O_3	Gd_2O_3	Tb_2O_3	Dy_2O_3	Ho_2O_3	Er_2O_3	Tm_2O_3	Yb_2O_3	Lu_2O_3	CaO	FeO	SrO	PbO	K_2O	SO_3	Total
mnz19-1	30.51	b.d.l.	0.41	6.53	0.53	b.d.l.	1.20	13.52	27.37	3.21	11.43	2.06	0.17	1.46	0.14	0.48	b.d.l.	0.40	b.d.l.	0.17	b.d.l.	1.38	b.d.l.	b.d.l.	0.10	b.d.l.	0.02	101.10
mnz20-1	28.89	b.d.l.	1.21	6.02	1.01	b.d.l.	1.04	13.36	27.34	3.21	11.57	2.11	b.d.l.	1.30	b.d.l.	0.39	b.d.l.	0.41	0.10	0.19	b.d.l.	0.55	b.d.l.	b.d.l.	0.12	b.d.l.	0.03	98.84
mnz21-1	30.23	b.d.l.	0.46	5.38	0.41	b.d.l.	1.02	13.79	27.68	3.27	12.11	2.18	0.16	1.60	0.15	0.51	b.d.l.	0.45	b.d.l.	0.18	b.d.l.	0.80	b.d.l.	b.d.l.	0.09	b.d.l.	0.03	100.50
mnz22-1	30.34	b.d.l.	0.35	6.51	0.57	b.d.l.	0.98	13.54	26.77	3.11	11.17	1.98	0.20	1.23	b.d.l.	0.29	b.d.l.	0.40	b.d.l.	0.16	b.d.l.	1.34	b.d.l.	0.04	0.12	0.02	0.03	99.13
mnz24-1	28.66	b.d.l.	1.69	6.44	0.84	b.d.l.	1.01	13.34	27.31	3.25	11.96	2.12	b.d.l.	1.38	b.d.l.	0.32	b.d.l.	0.51	0.10	0.17	b.d.l.	0.41	0.05	b.d.l.	0.11	b.d.l.	0.02	99.70
mnz25-1	28.14	b.d.l.	1.80	8.63	0.85	b.d.l.	0.52	13.45	27.24	3.16	11.58	1.89	b.d.l.	1.02	b.d.l.	0.23	b.d.l.	0.35	b.d.l.	0.14	b.d.l.	0.43	b.d.l.	b.d.l.	0.14	b.d.l.	b.d.l.	99.57
mnz26-1	28.40	b.d.l.	1.38	6.45	1.31	b.d.l.	0.80	13.88	27.69	3.06	10.83	1.79	0.16	1.03	0.09	0.26	b.d.l.	0.49	b.d.l.	0.17	b.d.l.	0.60	b.d.l.	b.d.l.	0.14	b.d.l.	b.d.l.	98.53
mnz27-1	28.71	b.d.l.	0.99	2.67	0.79	b.d.l.	0.61	14.69	29.19	3.31	12.47	2.12	b.d.l.	1.24	b.d.l.	0.22	b.d.l.	0.44	b.d.l.	0.15	b.d.l.	0.31	0.29	b.d.l.	0.07	0.03	b.d.l.	98.30
mnz28-1	29.00	b.d.l.	1.17	5.50	0.29	b.d.l.	1.07	13.62	27.84	3.20	11.84	2.28	b.d.l.	1.33	0.10	0.43	b.d.l.	0.42	b.d.l.	0.15	b.d.l.	0.26	b.d.l.	b.d.l.	0.08	b.d.l.	b.d.l.	98.56
mnz28-2	27.42	b.d.l.	2.11	9.44	0.61	b.d.l.	1.34	12.97	25.82	2.93	10.96	1.98	b.d.l.	1.34	0.13	0.47	b.d.l.	0.43	0.12	0.18	b.d.l.	0.35	0.19	b.d.l.	0.14	b.d.l.	0.03	98.98
mnz29-1	28.81	b.d.l.	1.55	6.28	0.88	b.d.l.	1.09	13.74	27.58	3.14	11.53	2.04	b.d.l.	1.25	0.08	0.23	b.d.l.	0.44	b.d.l.	0.19	b.d.l.	0.30	0.22	b.d.l.	0.12	0.01	0.02	99.52
mnz30-1	29.96	b.d.l.	0.73	3.87	0.65	b.d.l.	1.59	13.93	27.91	3.25	11.80	2.29	b.d.l.	1.52	0.10	0.56	b.d.l.	0.39	b.d.l.	0.19	b.d.l.	0.36	b.d.l.	b.d.l.	0.08	b.d.l.	0.03	99.20
SUD24/2																												
mnz1-1	30.48	b.d.l.	0.33	4.23	0.66	b.d.l.	0.33	13.58	28.62	3.43	12.76	2.13	0.29	1.01	b.d.l.	b.d.l.	b.d.l.	0.38	b.d.l.	0.13	b.d.l.	0.80	b.d.l.	0.11	0.08	0.03	b.d.l.	99.39
mnz1-2	30.57	b.d.l.	0.36	3.97	0.66	b.d.l.	0.35	13.33	28.58	3.54	13.06	2.11	0.28	1.03	b.d.l.	b.d.l.	b.d.l.	0.30	0.10	0.12	b.d.l.	0.76	b.d.l.	0.11	0.08	0.04	b.d.l.	99.35
mnz1-3	30.90	b.d.l.	0.36	4.58	0.72	b.d.l.	0.36	13.45	28.07	3.43	12.74	2.20	0.40	1.10	b.d.l.	b.d.l.	b.d.l.	0.36	0.09	0.13	b.d.l.	0.88	b.d.l.	0.12	0.10	0.05	0.02	100.06
mnz2	29.54	b.d.l.	0.93	12.63	0.67	b.d.l.	0.85	12.57	23.75	2.74	10.06	1.80	0.27	1.03	b.d.l.	0.22	b.d.l.	0.34	0.09	0.14	b.d.l.	2.13	0.38	0.05	0.19	0.06	0.02	100.46
mnz3	28.61	b.d.l.	1.60	13.96	0.69	b.d.l.	0.58	11.54	23.05	2.88	11.30	2.08	0.21	1.11	0.12	b.d.l.	b.d.l.	0.40	0.10	0.11	b.d.l.	1.73	0.54	b.d.l.	0.21	0.03	0.03	100.88
mnz5-1	29.18	b.d.l.	0.99	12.22	0.63	b.d.l.	0.60	10.05	24.21	3.20	12.55	2.52	0.16	1.22	b.d.l.	0.20	b.d.l.	0.39	0.12	0.17	b.d.l.	1.91	b.d.l.	b.d.l.	0.17	b.d.l.	b.d.l.	100.50
mnz5-2	29.40	b.d.l.	1.08	12.73	0.68	b.d.l.	0.59	9.88	23.78	3.12	12.35	2.62	0.18	1.29	b.d.l.	0.27	b.d.l.	0.34	b.d.l.	0.14	b.d.l.	1.99	b.d.l.	0.04	0.19	b.d.l.	b.d.l.	100.67
mnz5-3	29.70	b.d.l.	0.86	12.28	0.89	b.d.l.	0.74	9.87	23.27	3.14	12.39	2.53	0.20	1.33	0.08	b.d.l.	b.d.l.	0.41	b.d.l.	0.17	b.d.l.	2.20	b.d.l.	0.04	0.20	b.d.l.	0.04	100.35
mnz5-4	29.62	b.d.l.	0.93	11.66	0.84	b.d.l.	0.71	9.81	23.33	3.08	12.73	2.67	0.18	1.39	b.d.l.	0.27	b.d.l.	0.46	0.09	0.16	b.d.l.	1.98	b.d.l.	0.05	0.18	0.01	0.03	100.17
mnz6-1	29.75	b.d.l.	0.87	14.57	1.01	b.d.l.	0.72	8.97	21.70	2.93	12.13	2.64	0.25	1.54	0.09	0.25	b.d.l.	0.44	b.d.l.	0.11	b.d.l.	2.62	0.17	0.06	0.23	0.08	b.d.l.	101.15
mnz6-2	29.68	b.d.l.	0.99	16.37	0.91	b.d.l.	0.67	8.60	21.23	2.86	11.88	2.55	0.23	1.32	0.11	0.23	b.d.l.	0.38	b.d.l.	0.15	b.d.l.	2.88	0.16	0.05	0.25	0.05	0.03	101.58
mnz7-1	29.68	b.d.l.	0.41	6.25	0.68	b.d.l.	0.89	10.73	25.53	3.37	13.26	2.84	0.25	1.57	0.11	0.27	b.d.l.	0.41	b.d.l.	0.15	b.d.l.	1.28	0.15	b.d.l.	0.11	0.04	b.d.l.	97.99
mnz7-2	28.91	b.d.l.	0.57	7.14	0.76	0.03	0.78	9.95	24.36	3.32	13.78	2.95	0.17	1.62	0.14	0.31	b.d.l.	0.45	b.d.l.	0.20	b.d.l.	1.38	0.51	b.d.l.	0.13	0.05	b.d.l.	97.49
mnz9	30.51	b.d.l.	0.15	3.07	0.55	b.d.l.	0.97	17.68	29.81	3.06	9.50	1.17	0.30	0.78	0.11	0.33	b.d.l.	0.39	b.d.l.	0.26	b.d.l.	0.78	0.18	b.d.l.	0.07	0.03	b.d.l.	99.70
mnz12	29.70	b.d.l.	0.50	5.23	1.07	b.d.l.	0.70	11.53	26.41	3.45	14.00	3.00	0.22	1.83	0.10	0.22	b.d.l.	0.39	0.10	0.23	b.d.l.	1.01	0.30	b.d.l.	0.11	0.05	0.03	100.18
mnz18-1	29.78	b.d.l.	0.27	4.34	1.43	b.d.l.	0.90	10.83	26.01	3.37	14.21	3.18	0.16	1.77	0.11	0.34	b.d.l.	0.43	b.d.l.	0.18	b.d.l.	1.21	0.25	b.d.l.	0.11	0.04	b.d.l.	98.94
mnz18-2	30.86	b.d.l.	0.22	3.43	1.28	b.d.l.	1.12	11.56	26.60	3.49	13.76	3.08	0.24	1.82	0.10	0.37	b.d.l.	0.42	0.10	0.20	b.d.l.	0.94	0.42	b.d.l.	0.10	b.d.l.	b.d.l.	100.10
mnz18-3	30.72	b.d.l.	0.27	3.69	0.62	b.d.l.	0.75	11.69	27.34	3.63	14.29	2.95	0.14	1.68	0.14	0.31	b.d.l.	0.27	0.11	0.17	b.d.l.	0.75	0.52	b.d.l.	0.07	0.01	0.03	100.17
mnz20-1	30.30	b.d.l.	0.29	4.58	0.11	b.d.l.	0.30	14.77	30.01	3.22	10.88	1.17	0.17	0.24	b.d.l.	b.d.l.	b.d.l.	0.42	0.11	0.18	b.d.l.	0.84	0.14	0.04	0.07	0.10	b.d.l.	97.94
mnz21-1	30.26	b.d.l.	0.41	5.31	0.82	b.d.l.	0.90	11.90	26.66	3.55	13.67	2.88	0.18	1.48	b.d.l.	0.36	b.d.l.	0.39	b.d.l.	0.20	0.19	1.11	0.06	b.d.l.	0.10	b.d.l.	0.03	100.45

mnz21-2	30.48	b.d.l.	0.60	6.82	0.41	b.d.l.	0.75	11.82	26.44	3.28	13.17	2.60	0.25	1.32	b.d.l.	0.24	b.d.l.	0.40	0.10	0.16	b.d.l.	1.07	0.06	b.d.l.	0.10	b.d.l.	0.02	100.09
mnz21-3	29.79	b.d.l.	1.01	9.53	0.43	b.d.l.	0.60	11.39	25.47	3.16	12.08	2.53	b.d.l.	1.27	0.12	0.23	b.d.l.	0.43	b.d.l.	0.18	b.d.l.	1.32	0.14	b.d.l.	0.15	b.d.l.	0.03	99.85
mnz22-1	30.53	b.d.l.	0.42	3.49	0.98	0.04	0.77	12.86	28.51	3.45	12.78	2.50	0.18	1.12	b.d.l.	0.31	b.d.l.	0.29	b.d.l.	0.11	b.d.l.	0.85	0.30	b.d.l.	0.09	0.34	b.d.l.	99.90
mnz22-2	30.63	b.d.l.	0.53	4.59	1.12	b.d.l.	0.68	10.91	26.55	3.63	14.57	3.16	0.24	1.67	b.d.l.	b.d.l.	b.d.l.	0.31	b.d.l.	0.20	b.d.l.	0.89	0.28	b.d.l.	0.10	0.09	b.d.l.	100.15
mnz22-3	30.11	b.d.l.	0.36	3.17	0.97	b.d.l.	0.50	13.00	29.09	3.58	12.55	2.37	0.15	1.11	0.10	b.d.l.	b.d.l.	0.48	b.d.l.	0.11	b.d.l.	0.68	0.28	0.04	0.08	0.08	b.d.l.	98.81
mnz23-1	29.34	b.d.l.	0.97	9.88	1.36	b.d.l.	0.62	10.57	24.60	3.10	12.34	2.53	0.23	1.16	b.d.l.	0.22	b.d.l.	0.44	b.d.l.	0.19	b.d.l.	1.65	0.18	0.04	0.19	b.d.l.	0.02	99.65
mnz23-2	29.99	b.d.l.	0.56	6.67	0.76	b.d.l.	0.61	11.41	27.03	3.41	13.36	2.67	0.24	1.32	b.d.l.	0.20	b.d.l.	0.45	0.11	0.10	b.d.l.	1.25	0.10	b.d.l.	0.11	b.d.l.	b.d.l.	100.36
mnz23-5	29.78	b.d.l.	0.50	4.62	0.39	b.d.l.	0.46	12.62	28.51	3.47	12.93	2.47	b.d.l.	1.04	b.d.l.	0.19	b.d.l.	0.39	b.d.l.	0.17	b.d.l.	0.76	0.25	b.d.l.	0.07	0.04	b.d.l.	98.68
mnz23-6	29.63	b.d.l.	0.63	6.65	1.48	b.d.l.	0.84	11.13	25.67	3.24	13.09	2.68	0.24	1.47	0.12	0.24	b.d.l.	0.34	0.13	0.22	b.d.l.	1.31	0.18	b.d.l.	0.15	0.03	0.03	99.48
mnz23-7	29.87	b.d.l.	0.46	4.26	0.51	b.d.l.	0.54	11.96	27.77	3.56	13.30	2.73	0.22	1.27	b.d.l.	0.25	b.d.l.	0.29	b.d.l.	0.14	b.d.l.	0.72	0.29	b.d.l.	0.08	0.06	b.d.l.	98.27
mnz23-8	30.01	b.d.l.	0.26	3.69	1.14	b.d.l.	0.86	11.82	27.28	3.48	13.53	2.71	0.23	1.40	0.10	0.28	b.d.l.	0.30	b.d.l.	0.16	b.d.l.	1.00	0.29	b.d.l.	0.09	0.05	b.d.l.	98.69
mnz23-9	30.21	b.d.l.	0.43	5.09	0.69	0.14	0.77	11.05	26.47	3.46	13.91	3.01	0.18	1.54	0.08	0.31	b.d.l.	0.42	b.d.l.	0.17	b.d.l.	1.01	0.17	b.d.l.	0.09	0.08	0.03	99.31
mnz23-10	30.05	b.d.l.	0.29	3.83	1.26	b.d.l.	0.95	11.42	26.86	3.50	13.62	2.85	0.18	1.53	0.09	0.36	b.d.l.	0.44	b.d.l.	0.15	b.d.l.	1.05	0.12	b.d.l.	0.10	0.07	b.d.l.	98.72
mnz23-11	30.39	b.d.l.	0.39	4.30	0.62	b.d.l.	0.74	11.36	27.01	3.48	14.19	2.98	0.23	1.56	0.13	0.23	b.d.l.	0.41	b.d.l.	0.15	b.d.l.	0.87	0.15	b.d.l.	0.08	0.08	b.d.l.	99.34
mnz23-12	29.94	b.d.l.	0.54	3.90	1.26	b.d.l.	0.62	11.91	28.06	3.45	13.66	2.72	b.d.l.	1.29	b.d.l.	b.d.l.	b.d.l.	0.33	0.09	0.17	b.d.l.	0.82	0.28	b.d.l.	0.10	0.07	b.d.l.	99.22
mnz23-13	29.79	b.d.l.	0.61	3.82	0.89	b.d.l.	0.59	12.00	27.74	3.53	13.55	2.69	0.18	1.30	0.11	b.d.l.	b.d.l.	0.31	b.d.l.	0.17	b.d.l.	0.74	0.30	0.04	0.09	0.08	b.d.l.	98.54

Comments: all values are given in wt.%; b.d.l. – below detection limit.

Appendix 3.

Results of the LA-ICP-MS measurements of monazite from the mica schist SUD24/1

Analysis	Isotope ratio								Age (Ma) and discordance (%)							Concentration (ppm)		
	$^{207}Pb/^{235}U$	±2σ (abs)	$^{206}Pb/^{238}U$	±2σ (abs)	rho	$^{207}Pb/^{206}Pb$	±2σ (abs)	$^{206}Pb/^{204}Pb$	$^{207}Pb/^{235}U$	±2σ (abs)	$^{206}Pb/^{238}U$	±2σ (abs)	$^{207}Pb/^{206}Pb$	±2σ (abs)	disc§	Th	U	Pb
1	0.447	0.016	0.054	0.002	0.42	0.0602	0.0012	-22000	375	11	339	10	590	42	9.4	46300	12250	410
2	0.474	0.016	0.053	0.002	0.49	0.0646	0.0011	-65000	393	11	335	9	740	37	14.7	87200	9540	759
3	0.572	0.021	0.054	0.002	0.48	0.0765	0.0016	-105000	457	13	341	9	1084	41	25.5	88500	9910	787
4	0.508	0.020	0.054	0.002	0.31	0.0677	0.0018	40000	415	14	340	10	816	57	18.0	125400	4320	1078
5	0.471	0.021	0.054	0.002	0.29	0.0646	0.0021	24000	391	14	338	11	720	70	13.6	163600	6070	1359
6	0.396	0.016	0.052	0.002	0.44	0.0548	0.0013	-10000	337	11	330	10	374	54	2.3	101900	5010	861
7	0.475	0.016	0.054	0.002	0.39	0.0643	0.0011	40000	394	11	337	9	728	38	14.5	89600	10390	799
8	0.459	0.016	0.053	0.002	0.41	0.0628	0.0011	-130000	383	11	335	9	680	38	12.7	127900	21470	1122
9	0.500	0.017	0.054	0.002	0.51	0.0673	0.0012	-42000	411	12	340	9	830	36	17.3	95800	11180	869
10	0.560	0.019	0.054	0.002	0.43	0.0749	0.0013	-55000	451	13	342	10	1046	36	24.1	110500	11710	990
11	0.381	0.014	0.052	0.002	0.40	0.0528	0.0010	54000	328	10	328	9	302	42	-0.2	43910	7380	383
12	0.383	0.014	0.052	0.002	0.33	0.0532	0.0011	38000	329	10	330	9	314	46	-0.2	54800	9010	469
13	0.384	0.013	0.052	0.002	0.30	0.0535	0.0011	15000	329	10	328	9	330	45	0.3	45200	7750	386

Comments: § disc. = $\{1 - [(^{206}Pb/^{238}U) / (^{207}Pb/^{235}U)]\} \times 100$ for monazite younger than 1 Ga; disc. = $\{1 - [(^{206}Pb/^{238}U) / (^{207}Pb/^{206}Pb)]\} \times 100$ for monazite older than 1 Ga.

Appendix 4.

Results of the monazite EPMA dating in the mica schist SUD24/2 with concentrations of Th, U, Pb and Y

Analysis	Th (wt.%)	2σ	U (wt.%)	2σ	Pb (wt.%)	2σ	Y (wt.%)	Th* (wt.%)	Age (Ma)	2σ
mnz1-1	3.71	0.04	0.61	0.01	0.08	0.01	0.26	5.73	328	46
mnz1-2	3.49	0.04	0.61	0.01	0.07	0.01	0.27	5.50	306	48
mnz1-3	4.02	0.04	0.67	0.01	0.09	0.01	0.29	6.23	342	42
mnz2	11.10	0.08	0.66	0.01	0.20	0.01	0.67	13.37	342	22
mnz3	12.27	0.09	0.68	0.01	0.22	0.01	0.45	14.62	342	21
mnz5-1	10.74	0.08	0.62	0.01	0.18	0.01	0.47	12.86	318	23
mnz5-2	11.19	0.08	0.67	0.01	0.20	0.01	0.46	13.47	329	22
mnz5-3	10.79	0.08	0.85	0.02	0.20	0.01	0.58	13.67	335	22
mnz5-4	10.24	0.08	0.80	0.01	0.19	0.01	0.56	12.95	329	23
mnz6-1	12.81	0.09	0.97	0.02	0.24	0.01	0.57	16.11	338	19
mnz6-2	14.38	0.10	0.89	0.02	0.26	0.01	0.53	17.43	339	18
mnz7-1	5.50	0.05	0.64	0.01	0.11	0.01	0.70	7.64	331	35
mnz7-2	6.28	0.05	0.71	0.01	0.13	0.01	0.62	8.65	335	31
mnz9	2.69	0.03	0.50	0.01	0.07	0.01	0.76	4.36	344	59
mnz12	4.59	0.04	0.98	0.02	0.11	0.01	0.55	7.83	329	34
mnz18-1	3.82	0.04	1.29	0.02	0.11	0.01	0.71	8.05	313	34
mnz18-2	3.02	0.03	1.15	0.02	0.10	0.01	0.88	6.78	332	40
mnz18-3	3.25	0.03	0.57	0.01	0.07	0.01	0.59	5.11	323	51
mnz20-1	4.02	0.04	0.14	0.01	0.07	0.01	0.23	4.51	342	57
mnz21-1	4.67	0.04	0.75	0.01	0.10	0.01	0.71	7.17	310	37
mnz21-2	6.00	0.05	0.40	0.01	0.11	0.01	0.59	7.35	326	37
mnz21-3	8.37	0.07	0.43	0.01	0.15	0.01	0.47	9.84	350	29
mnz22-1	3.06	0.03	0.93	0.01	0.09	0.01	0.60	6.12	317	43
mnz22-2	4.04	0.04	1.02	0.02	0.11	0.01	0.53	7.40	321	36
mnz22-3	2.79	0.03	0.88	0.01	0.08	0.01	0.40	5.68	314	46
mnz23-1	8.69	0.07	1.25	0.02	0.19	0.01	0.49	12.85	334	23
mnz23-2	5.87	0.05	0.71	0.01	0.11	0.01	0.48	8.23	307	33
mnz23-5	4.06	0.04	0.37	0.01	0.07	0.01	0.36	5.32	290	49
mnz23-6	5.84	0.05	1.35	0.02	0.15	0.01	0.66	10.28	329	27
mnz23-7	3.74	0.04	0.48	0.01	0.08	0.01	0.42	5.33	329	49
mnz23-8	3.24	0.03	1.03	0.02	0.09	0.01	0.68	6.62	316	40
mnz23-9	4.47	0.04	0.65	0.01	0.09	0.01	0.61	6.62	303	40
mnz23-10	3.37	0.03	1.15	0.02	0.10	0.01	0.75	7.12	325	37
mnz23-11	3.77	0.04	0.58	0.01	0.08	0.01	0.58	5.71	319	46
mnz23-12	3.43	0.04	1.14	0.02	0.10	0.01	0.49	7.18	324	37
mnz23-13	3.36	0.03	0.81	0.01	0.09	0.01	0.47	6.04	323	43

Comments: Th* values denote measured Th plus U converted to hypothetical Th with respect to production of the equivalent amount of radiogenic Pb (Konečný et al., 2018)